ISOTOPE SHIFTS AND FINE STRUCTURE OF Li D LINES AND DETERMINATION OF ^{6,7}Li RELATIVE NUCLEAR CHARGE RADIUS

GEORGE A. NOBLE

A DISSERTATION SUBMITTED TO THE FACULTY OF GRADUATE STUDIES

IN PARTIAL FULFILMENT OF THE REQUIREMENTS
FOR THE DEGREE OF

DOCTOR OF PHILOSOPHY

GRADUATE PROGRAM IN PHYSICS AND ASTRONOMY
YORK UNIVERSITY
TORONTO, ONTARIO
APRIL 2009

ISOTOPE SHIFTS AND FINE STRUCTURE OF Li D LINES AND DETERMINATION OF ^{6,7}Li RELATIVE NUCLEAR CHARGE RADIUS

by **George A. Noble**

a dissertation submitted to the Faculty of Graduate Studies of York University in partial fulfilment of the requirements for the degree of

DOCTOR OF PHILOSOPHY

ISOTOPE SHIFTS AND FINE STRUCTURE OF Li D LINES AND DETERMINATION OF ^{6,7}Li RELATIVE NUCLEAR CHARGE RADIUS

by **George A. Noble**

Examination Committee Members:

1. J. Darewych
2. M. De Robertis
3. R. Fournier
4. G. W. Harris
5. H. K. Haugen
6. S. Menary
7. W. A. van Wijngaarden

Abstract

The lithium D lines were studied using a dye laser that was frequency modulated by an electro-optic modulator to excite an atomic beam. The modulation frequency was specified by a frequency synthesizer to an accuracy of a few parts in 10^7. The transmission of part of the laser beam through an etalon was monitored to check for any nonlinearity of the laser scan. Fluorescence, produced by the radiative decay of the excited state, was detected by a photomultiplier and recorded as the laser frequency was scanned across the resonance. Hence, each transition was multiply excited allowing for convenient calibration of the laser frequency scan.

The ^{6,7}Li 2P fine structure intervals were found to be $10,052.964 \pm 0.050$ and $10,053.119 \pm 0.058$ MHz which is about 2 MHz higher than the most reliable results calculated using Hylleraas Variational theory. This has motivated efforts to take higher order effects into consideration to improve the theoretical estimates. The D1 and D2 isotope shifts were determined to be $10,534.039 \pm 0.070$ and $10,534.194 \pm 0.104$ MHz. These two results yielded consistent values for the relative nuclear charge radius squared $\Delta {R_c}^2$ of ^{6,7}Li. The average result of 0.755 ± 0.023 fm^2 for $\Delta {R_c}^2$ agreed very well with values found by other experiments that studied the Li^+ 1s2s ^{3}S $\rightarrow$ 1s2p ^{3}P and the Li $2S_{1/2} \rightarrow 3S_{1/2}$ transitions. The relative nuclear charge radius was found with an uncertainty of only several millifermi (10^{-18} meter) which is more than an order of magnitude smaller than obtained using electron scattering.

Acknowledgements

I thank my supervisor William van Wijngaarden for encouraging me to learn and solve problems. I admire his dedication to research and teaching. He was generous with his support, valuable advice and time. William helped me meet one of my goals - to make a significant contribution to the atomic physics field. I also thank my committee members for their comments and advice.

There are many people at York who I wish to acknowledge. The technical staff have been extremely helpful. In particular, I appreciate Ator Sarkisoff for his assistance in machining and Jim Hodges for helping repair electronic equipment. In the lab, Baolong Lu showed me persistence needed for experimental physics. I have enjoyed working with Brad Schultz on experiments. I value Yiannis Haranas for his support and friendship.

I give thanks to my parents Arnold and Betty Noble for their love and support. My late father would have been very proud to see me graduate. I appreciate my brother Andrew and his wife Sandi for their encouragement. I am grateful to my fiancée Lily for all her love.

This work was supported by the Natural Science and Engineering Council of Canada. Finally, I thank York University and the Ontario Graduate Scholarship in Science and Technology Program for financial assistance.

Table of Contents

List of Tables

List of Figures

1 Introduction

1.1 Motivation

Lithium has a number of properties making it useful for both experimental and theoretical study. It has a relatively low melting point of 180 °C that facilitates the generation of an atomic beam. It also has transitions at visible wavelengths where continuous wave dye and diode lasers readily operate which facilitates the application of precise laser spectroscopic techniques. Lithium has two stable and three radioactive isotopes as shown in Table 1.1. Finally, lithium is one of the simplest atoms to model as it has only 3 electrons. This permits the study of QED effects such as the Lamb shift which scales to lowest order as $Z^4\alpha^5 \ln(Z\alpha)mc^2$ where Z is the nuclear charge, α is the fine structure constant, m is the electron mass and c is the speed of light.

Table 1.1: Lithium Isotopes

Isotope	Natural Abundance	Nuclear Spin	Lifetime (msec)
^{6}Li	7.5%	1	
^{7}Li	92.5%	3/2	
^{8}Li		2	836 ± 6[1]
^{9}Li		3/2	178.3 ±0.4[1]
^{11}Li		3/2	8.59 ±0.14[2]

In recent years, there have been a number of developments improving our understanding of lithium. Various precise measurements of fine structure and isotope shifts have been made using the Li^+ 1s2s $^3S \rightarrow$ 1s2p ^3P transition, the Li D lines and the Li $2S_{1/2} \rightarrow 3S_{1/2}$ transition [3–18]. Not all of the experiments have yielded consistent results [19]. Substantial theoretical progress has also been made using the Hylleraas Variational technique [20]. The combination of high precision experiment and theory can determine the relative nuclear charge radius of the various lithium isotopes. This led to the discovery of so called halo neutrons in the case of ^{11}Li [21]. The results for the relative nuclear radii are more than an order of magnitude more accurate than data produced by electron scattering experiments [22, 23].

This work determined the fine structure splitting of the neutral ^{6,7}Li 2P state as well as the isotope shift of the D1 and D2 transitions. The results are substantially more accurate than previous measurements. The ^{6,7}Li relative nuclear charge radius found using the D1 and D2 transitions were consistent with each other and also agreed with data obtained from the most accurate experiments studying the Li^+ 1s2s $^3S \rightarrow$ 1s2p ^3P transition and the Li $2S_{1/2} \rightarrow 3S_{1/2}$ transitions. This enabled the relative ^{6,7}Li nuclear charge radius to be found with an uncertainty of only several millifermi (10^{-18} meter).

1.2 Lithium Energy Levels

The lithium D lines arise from transitions between the $2S_{1/2}$ ground and $2P_{1/2,3/2}$ excited states as shown in Fig. 1.1. The ground and excited states are split into various levels labelled by the hyperfine quantum number F which is the sum of the total electron angular momentum and the nuclear spin. The hyperfine interaction depends on the nuclear spin which is given in Table 1.1. The energies of the hyperfine levels were calculated using the most accurate hyperfine data available in the literature [11, 24]. This experiment determined the ^{6,7}Li 2P fine structure intervals and D1 and D2 isotope shifts defined in Fig. 1.1. These intervals are defined relative to the center of gravity of the $2P_{1/2,3/2}$ states.

The natural linewidth of the D lines derived from the lifetime of the 2P state is 5.8 MHz [25, 26]. This is larger than the hyperfine splittings of the $2P_{3/2}$ state in ^{6}Li and comparable to those found in ^{7}Li. Hence, in Fig. 1.1, transitions 5 and 6 in ^{6}Li as well as 11 and 12 in ^{7}Li are not drawn to any particular hyperfine level of the excited $2P_{3/2}$ state as the laser excites multiple hyperfine levels. In this experiment, the laser frequency was scanned across the $2S \rightarrow 2P$ resonance. The D1 line consists of the four transitions labelled 1 to 4 in ^{6}Li and 7 to 10 in ^{7}Li. The D2 line consists of the two transitions labelled 5 and 6 in ^{6}Li and 11 and 12 in ^{7}Li.

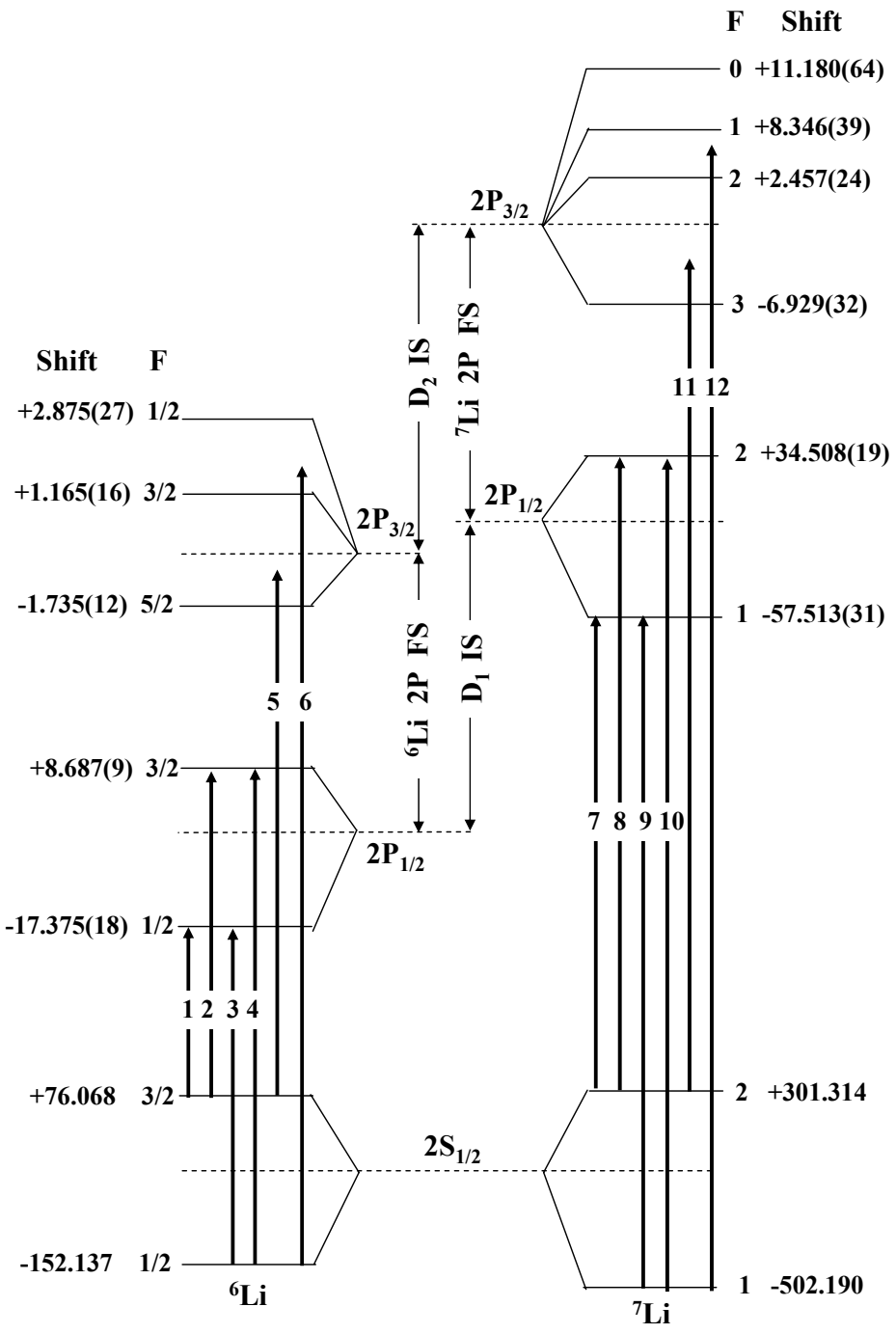

Figure 1.1: Relevant Lithium Energy Levels. The vertical energy axis is not drawn to scale. The positions of the various hyperfine levels are indicated relative to the center of gravity energy of a state $E_{cg} = \Sigma_F(2F+1)E_F/\Sigma_F(2F+1)$. All units are in MHz where the uncertainty of the energy level is given in brackets.

1.3 Fine Structure

The fine structure results from relativistic perturbations of the atom's Hamiltonian [27, 28]. For simplicity, its origin is discussed for a hydrogenic atom. The largest terms in the Hamiltonian are given by the following.

$$H_0 = \frac{p^2}{2\mu} - \frac{Ze^2}{r} \tag{1.1}$$

Here, the first term represents the electron's kinetic energy where p is the electron momentum and μ is its reduced mass defined by

$$\frac{1}{\mu} = \frac{1}{m} + \frac{1}{M_{nuc}} \tag{1.2}$$

where m is the electron mass and M_{nuc} is the mass of the nucleus. The second term in equation 1.1 is the Coulomb interaction between the nucleus with electric charge $+Ze$ and the electron with charge $-e$ where r is the distance between the electron and the nucleus.

There are three terms that contribute to the fine structure. The first term arises from the relativistic kinetic energy defined by

$$H_{rel} = \sqrt{p^2c^2 + (mc^2)^2} - mc^2 - \frac{p^2}{2m} \tag{1.3}$$

where p is the electron momentum and c is the speed of light. Taking the leading terms in the expansion of H_{rel} in powers of (p/mc) gives the following.

$$H_{rel} = -\frac{p^4}{8m^3c^2} \tag{1.4}$$

The second contribution to the fine structure arises from interaction of the electron magnetic moment with the magnetic field generated by a moving nucleus as viewed by the electron. This spin orbit interaction is given by

$$H_{so} = -\frac{1}{2}\frac{Ze^2}{m^2c^2r^3}\vec{L}\cdot\vec{S} \tag{1.5}$$

where $\vec{L}$ is the orbital angular momentum of the electron and $\vec{S}$ is the electron's spin. The third contribution to the fine structure is the so called Darwin term which arises from the Dirac equation and is given by the following.

$$H_D = \frac{\hbar^4}{8m^3c^2}\nabla^2 V(r) \tag{1.6}$$

Here $\hbar$ is Planck's constant divided by 2π and $V(r)$ is the electrostatic potential generated by the nucleus as a function of the distance r. The Darwin term contributes only to S states for which the electron wavefunction does not vanish at the nucleus. The fine structure energy is the sum of these three contributions

$$E_{FS} = E_{rel} + E_{so} + E_D \tag{1.7}$$

which simplifies to the following.

$$\frac{E_{FS}}{E_n} = \left(\frac{Z\alpha}{n}\right)^2\left(\frac{n}{j+1/2} - \frac{3}{4}\right) \tag{1.8}$$

where E_n is the solution of the nonrelativistic Hamiltonian given by equation 1.1. n is the principal quantum number and j is the total electron angular momentum quantum number.

For a multielectron atom such as lithium, analytic solutions of the Schrodinger equation using the nonrelativistic Hamiltonian do not exist. Numerical techniques to compute the electron wavefunctions have therefore been developed as described in section 1.5. These wavefunctions are then used to evaluate the fine structure.

1.4 Isotope Shift

The nonrelativistic Hamiltonian describing an atom consisting of a nucleus at position $\vec{r}_{nuc}$ and N electrons at positions $\vec{r}_i$ where $i = 1, 2, 3...N$ is given by the following expression [29–31].

$$H(\vec{r}_{nuc}, \vec{r}_i, \vec{p}_{nuc}, \vec{p}_i) = \frac{{p_{nuc}}^2}{2M_{nuc}} + \sum_i \frac{{p_i}^2}{2m} + \sum_i V_{eN}(|\vec{r}_i - \vec{r}_{nuc}|) + \sum_{i<j} V_{ee}(|\vec{r}_i - \vec{r}_j|) \quad (1.9)$$

Here, $\vec{p}_{nuc}$ and $\vec{p}_i$ are the linear momenta of the nucleus and electrons respectively. V_{eN} describes the Coulomb interaction between the electrons and the nucleus while V_{ee} describes the repulsion of the electrons with each other. The center of mass $\vec{R}_{CM}$ is given by

$$M_{tot}\vec{R}_{CM} = M_{nuc}\vec{r}_{nuc} + m\sum_i \vec{r}_i \quad (1.10)$$

where $M_{tot} = M_{nuc} + Nm$ is the atom's total mass. The electron position measured with respect to the nucleus is defined by $\vec{\rho}_i = \vec{r}_i - \vec{r}_{nuc}$. The canonical momenta $\vec{\pi}_i$

and $\vec{P}_{CM}$ corresponding to $\vec{\rho}_i$ and $\vec{R}_{CM}$ are as follows.

$$\begin{aligned} \vec{p}_i &= \vec{\pi}_i + \frac{m}{M_{tot}}\vec{P}_{CM} \\ \vec{p}_{nuc} &= -\sum_i \vec{\pi}_i + \frac{M_{nuc}}{M_{tot}}\vec{P}_{CM} \end{aligned} \tag{1.11}$$

The Hamiltonian then becomes

$$H(\vec{\rho}_i, \vec{\pi}_i) = \sum_i \frac{{\pi_i}^2}{2\mu} + \frac{1}{M_{tot}}\sum_{i<j} \vec{\pi}_i \cdot \vec{\pi}_j + \sum_i V_{eN}(\rho_i) + \sum_{i<j} V_{ee}(|\vec{\rho}_i - \vec{\rho}_j|) \tag{1.12}$$

where the term $P_{CM}^2/2M_{tot}$ describing the kinetic energy of the moving atom has been omitted. The first two terms obviously depend on the nuclear mass and hence are different for various isotopes. The resulting isotope shift of a transition E_{ISO} generated by the first term is called the normal mass shift E_{NMS} while the second term generates the so called specific mass shift E_{SMS}.

An additional contribution to the isotope shift arises from the dependence of the nuclear size on the number of neutrons. This can be understood by considering the nucleus to be a uniformly charged sphere of radius R. The electrostatic potential generated by such a nucleus located at the origin is given by the following.

$$V(r) = \begin{cases} -\dfrac{Ze}{2R}\left(3 - \dfrac{r^2}{R^2}\right) & r \leq R \\ -\dfrac{Ze}{r} & r > R \end{cases} \tag{1.13}$$

A change ΔR in the nuclear size changes the potential an amount

$$\Delta V = \frac{3Ze}{2R^2}\left(1 - \frac{r^2}{R^2}\right)\Delta R \tag{1.14}$$

The nuclear size can also be defined in terms of the charge distribution. One commonly refers to the root mean square charge radius R_c defined as

$$R_c^2 = \frac{1}{Ze} \int r^2 \rho(r) dV \tag{1.15}$$

where ρ is the electric charge density of the nucleus. One can show that ${R_c}^2 = \frac{3}{5}R^2$ for the uniform charge distribution considered above. ΔV can be expressed as follows

$$\Delta V = \frac{5Ze}{4R^3} \left(1 - \frac{r^2}{R^2}\right) \Delta {R_c}^2 \tag{1.16}$$

Evaluating the expectation value of ΔV using the electron wavefunction at the nucleus shifts the energy by an amount called the field shift given by

$$E_{Field\ Shift} = C\Delta {R_c}^2 \tag{1.17}$$

where C is a constant calculated using the electron wavefunction. One can show this expression also results for other than uniform nuclear charge distributions [29]. Hence, the isotope shift E_{ISO} is given by

$$E_{ISO} = E_{NMS} + E_{SMS} + E_{Field\ Shift} \tag{1.18}$$

The challenge for theorists is to compute very accurate wavefunctions corresponding to the Hamiltonian that consists of the nonrelativistic kinetic energy of the electrons and the Coulomb interactions in the atom. These wavefunctions are then used to compute the mass shift terms of the isotope shift as well as the constant C. The

relative nuclear charge radius can then be found from an experimental measurement of the isotope shift.

1.5 Hylleraas Variational Method

The Hylleraas Variational Method has been very useful to find the energies of states in few electron atoms to very high accuracy [20, 30, 32, 33]. This method uses a trial wavefunction that depends on various parameters. An upper bound is placed on the state energy by varying the parameters. The choice of the wavefunction and the number of parameters determine how close the result is to the actual state energy.

The advent of computers greatly increased the number of parameters that could be used. The group led by G. W. F. Drake considered a trial wavefunction for lithium

$$\begin{aligned} \Psi(\vec{\rho}_1, \vec{\rho}_2, \vec{\rho}_3) &= \sum_{j_1,j_2,j_3,j_{12},j_{13},j_{23}} a_{j_1,j_2,j_3,j_{12},j_{13},j_{23}}\ \rho_1^{j_1}\ \rho_2^{j_2}\ \rho_3^{j_3}\ \rho_{12}^{j_{12}}\ \rho_{13}^{j_{13}}\ \rho_{23}^{j_{23}} \\ &\times\ e^{-\alpha\rho_1-\beta\rho_2-\gamma\rho_3}\ Y(\hat{\rho}_1, \hat{\rho}_2, \hat{\rho}_3)\ \chi(1,2,3) \end{aligned} \quad (1.19)$$

where $a_{j_1,j_2,j_3,j_{12},j_{13},j_{23}}$ as well as α, β and γ are the variational coefficients. Y is a linear combination of spherical harmonic functions for the three electrons that depends on the various angular coordinates while χ represents the electron spin. Y and χ are defined such that the wavefunction is antisymmetrized with respect to exchange of any two electrons to satisfy the Pauli Exclusion Principle. These wavefunctions are used to perturbatively evaluate corrections due to relativistic effects, QED as well as

the hyperfine interaction.

The Hylleraas Variational method has been very successful in computing fine and hyperfine structure intervals in two electron systems such as He and Li^+ [5, 6, 20]. The amount of computations required increases exponentially with the number of electrons. Hence, only recently has this technique been utilized to study neutral lithium. Table 1.2 lists the values of the mass shift calculated for transitions for which isotope shift measurements have been made. The mass shift equals the sum of the normal and specific mass shift terms discussed in Section 1.4 and C appears in the field shift term of the isotope shift. The initial calculations by Drake and collaborators [20] were recently refined to include higher order relativistic effects [34]. Their latest value for the mass shift is nearly identical with that found previously by the independent theoretical group of Puchalski for the Li $2\ ^2S_{1/2} \rightarrow 3\ ^2S_{1/2}$ transition [35].

Table 1.2: Calculated Mass Shift and Dependence on Nuclear Size

Transition	Mass Shift (MHz)	C (MHz/fm^2)	Reference
Li^+ $2\ ^3S_1 \rightarrow 2\ ^3P_0$	$34,740.17 \pm 0.03$	9.705	[20]
Li^+ $2\ ^3S_1 \rightarrow 2\ ^3P_1$	$34,739.87 \pm 0.03$	9.705	[20]
Li^+ $2\ ^3S_1 \rightarrow 2\ ^3P_2$	$34,742.71 \pm 0.03$	9.705	[20]
Li $2\ ^2S_{1/2} \rightarrow 2\ ^2P_{1/2}$	$10,532.17 \pm 0.07$	2.457	[20]
	$10,532.111 \pm 0.006$		[34]
Li $2\ ^2S_{1/2} \rightarrow 2\ ^2P_{3/2}$	$10,532.57 \pm 0.07$	2.457	[20]
	$10,532.506 \pm 0.006$		[34]
Li $2\ ^2S_{1/2} \rightarrow 3\ ^2S_{1/2}$	$11,453.010 \pm 0.056$	1.5661	[17]
	$11,452.822 \pm 0.002$	1.5732	[35]
	$11,452.821 \pm 0.002$		[34]

2 Review of Previous Work

Lithium isotope shift data have been obtained by a number of experiments for the Li^+ 1s2s $^3S_1 \rightarrow$ 1s2p $^3P_{0,1,2}$ transitions, the Li D1 and D2 lines as well as the for the two photon transition Li 2 $^2S_{1/2} \rightarrow$ 3 $^2S_{1/2}$. These transitions occur at optical wavelengths where narrow linewidth lasers facilitate precision measurements. For each of the aforementioned transitions, experiments that have reported isotope shift and fine structure splitting data having accuracies of better than 1 MHz are reviewed.

2.1 Li^+ 1s2s $^3S \rightarrow$ 1s2p ^3P Transition

The two electron system, Li^+, is well understood theoretically. The 1s2s $^3S \rightarrow$ 1s2p ^3P transition shown in Fig. 2.1, occurs at 548 nm making it accessible to precision laser spectroscopy. The Li^+ 1s2s ^3S state has a lifetime of nearly one minute [36]. Typically, metastable lithium ions are generated by first heating lithium in an oven to a temperature of about 500 °C. The neutral atoms are then bombarded with an electron beam. The resulting ions are collimated by an electrostatic lens and accelerated. Li^+ currents of 1 μA can be generated where about 0.1% of the ions occupy the metastable state [6].

The experiment of Riis et al [5], illustrated in Fig. 2.2, used the so called laser ion beam (LIB) excitation method to measure the isotope shift of the $^{6,7}Li^+$ 1s2s $^3S_1 \rightarrow$ 1s2p $^3P_{0,1,2}$ transitions. The 100 keV metastable Li^+ beam was excited by two dye

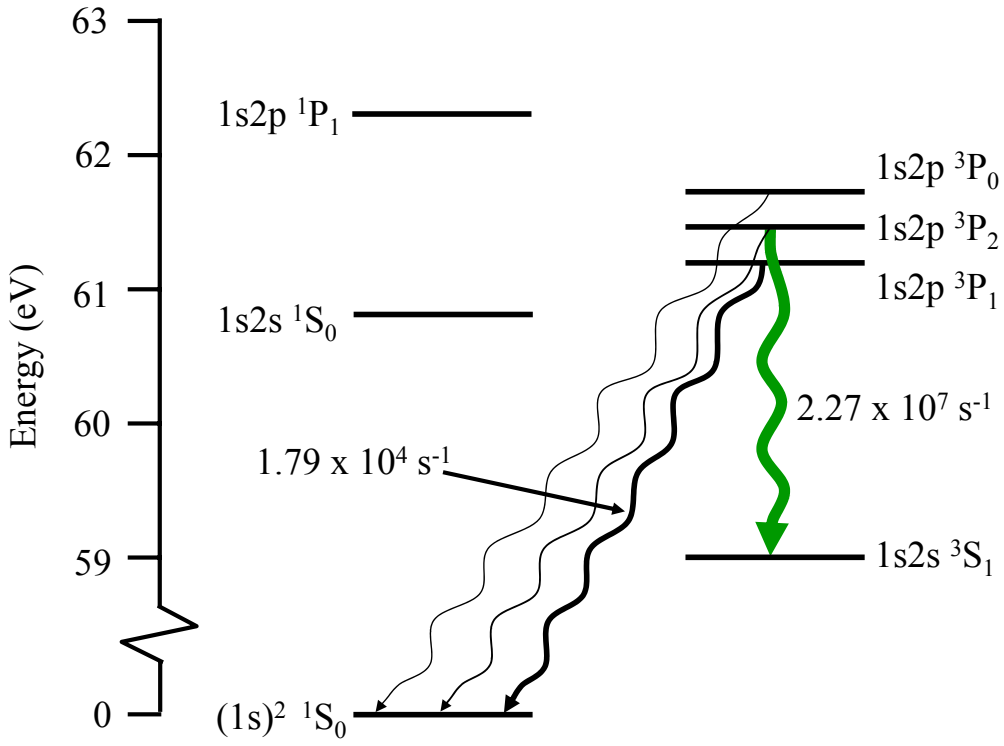

Figure 2.1: Li^+ Energy Levels

lasers. A saturation spectroscopy signal was obtained by having the two laser beams propagate parallel and antiparallel with the ions. The dye laser copropagating with the ion beam was Doppler tuned into resonance with one of the $^{6,7}Li^+$ 1s2s $^3S_1 \rightarrow$ 1s2p $^3P_{0,1,2}$ transitions by slightly varying the ion acceleration voltage. The second dye laser, counter-propagating with the ions, was scanned across the resonance using an acousto-optic modulator (AOM). A photomultiplier (PMT) detected a fluorescence signal consisting of a 25 MHz FWHM Lamb dip superimposed on a 100 MHz FWHM Doppler broadened peak. The Lamb dip signal was isolated by subtracting

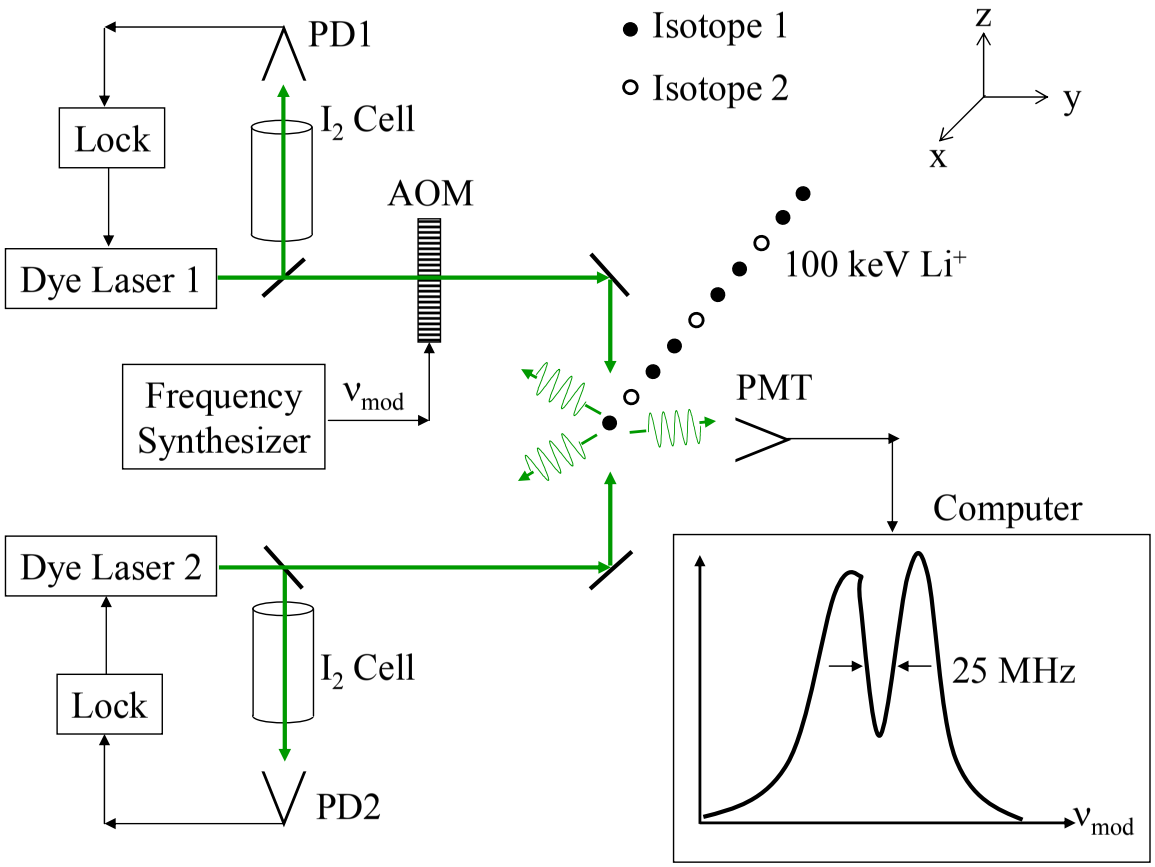

Figure 2.2: Apparatus for Laser Excitation of Metastable Li Ion Beam used by Riis et al

the Doppler broadened signal obtained when the first dye laser was blocked. Absolute frequencies of both dye lasers were found using a wavemeter not shown in Fig. 2.2 and a Fabry Perot etalon whose length was locked using an iodine stabilized HeNe laser. The $^{6,7}Li^{+}$ isotope shifts were determined for the 1s2s $^{3}S_{1} \rightarrow$ 1s2p $^{3}P_{0,1,2}$ transitions with an uncertainty of 0.6 MHz.

2.2 Li D Lines

A number of experiments have measured the fine structure splittings and isotope shifts of the neutral D lines. The earliest investigations used lamps to generate resonant light at 670 nm. A number of techniques were developed to achieve a resolution smaller than the Doppler width. The most recent work has used narrow linewidth dye and diode lasers. The resolution of these later experiments is limited by the 5.8 MHz, FWHM natural linewidth of the D lines [25, 26] and the hyperfine splitting of the excited $2P_{1/2,3/2}$ states [24].

2.2.1 Level Crossing

One of the first high precision determinations of the ^{6,7}Li 2P fine structure was done using the Level Crossing (LC) technique [7]. Atoms were excited by light linearly polarized along the direction of an applied magnetic field. Fluorescence, produced by the radiative decay of the excited state, was then detected. The magnetic field

shifted the energies of the Zeeman sublevels. At certain values of the magnetic field, the Zeeman sublevels of different fine structure levels were degenerate. This caused a change in the ratio of vertical to horizontal linearly polarized fluorescence.

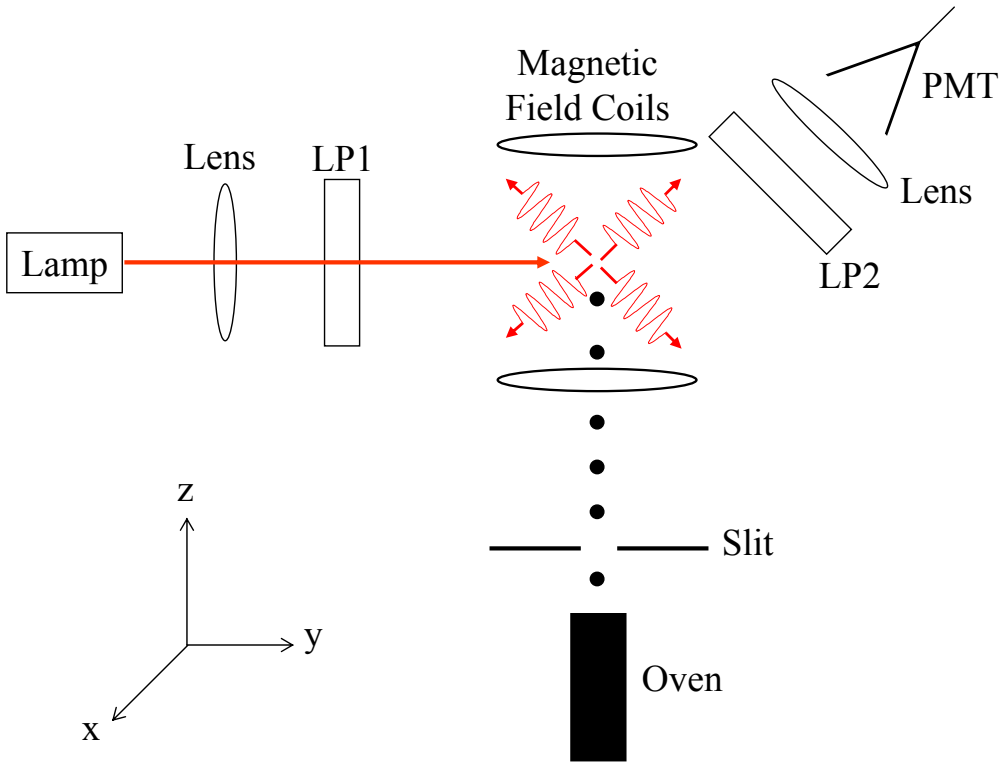

Figure 2.3: Level Crossing Apparatus used by Brog et al

The experiment by Brog et al is illustrated in Fig. 2.3. An atomic beam was generated by heating lithium metal in an oven to a temperature of about 420 °C. Isotopically enriched lithium metal was used to separately generate beams of ^{6}Li or ^{7}Li. A single slit was used to weakly collimate the atoms propagating in the

z direction. The background pressure was only about 1 millitorr. Argon gas was used to prevent the lithium vapor from collecting on the vacuum chamber windows. Atoms were excited to the 2P state using light produced by an rf discharge lamp. Light directed along the y axis was first collimated by a lens and then passed through a linear polarizer LP1. A magnetic field of up to several kG was generated in the z direction by a pair of Helmholtz coils. Fluorescence emitted along the -x axis was focussed by a lens onto a photomultiplier (PMT). This light first passed through a linearly polarizer (LP2) oriented such that the transmission axis was either parallel or perpendicular to the magnetic field.

The fluorescence polarization was measured as a function of the magnetic field. The fine structure interval was extracted from the observed level crossing field and using the Landé factor as well as the magnetic dipole and the electric quadrupole hyperfine constants of the $2P_{1/2,3/2}$ states. The 2P fine structure splittings were found to be 10,052.76 $\pm$ 0.22 and 10,053.24 $\pm$ 0.22 MHz for ^{6}Li and ^{7}Li respectively. The uncertainty was largely due to the accuracy of the magnetic field measurement.

2.2.2 Optical Double Resonance

The ^{7}Li 2P fine structure has also been determined using the optical double resonance (ODR) technique [12]. Atoms experiencing a uniform magnetic field were first excited by linearly polarized light to a Zeeman sublevel of the excited $2P_{1/2}$ state. A radio frequency was next applied that caused transitions among the Zeeman sublevels

of the $2P_{1/2}$ and $2P_{3/2}$ states. This transition can be monitored by detecting a change in the polarization of fluorescence emitted when the excited state radiatively decays.

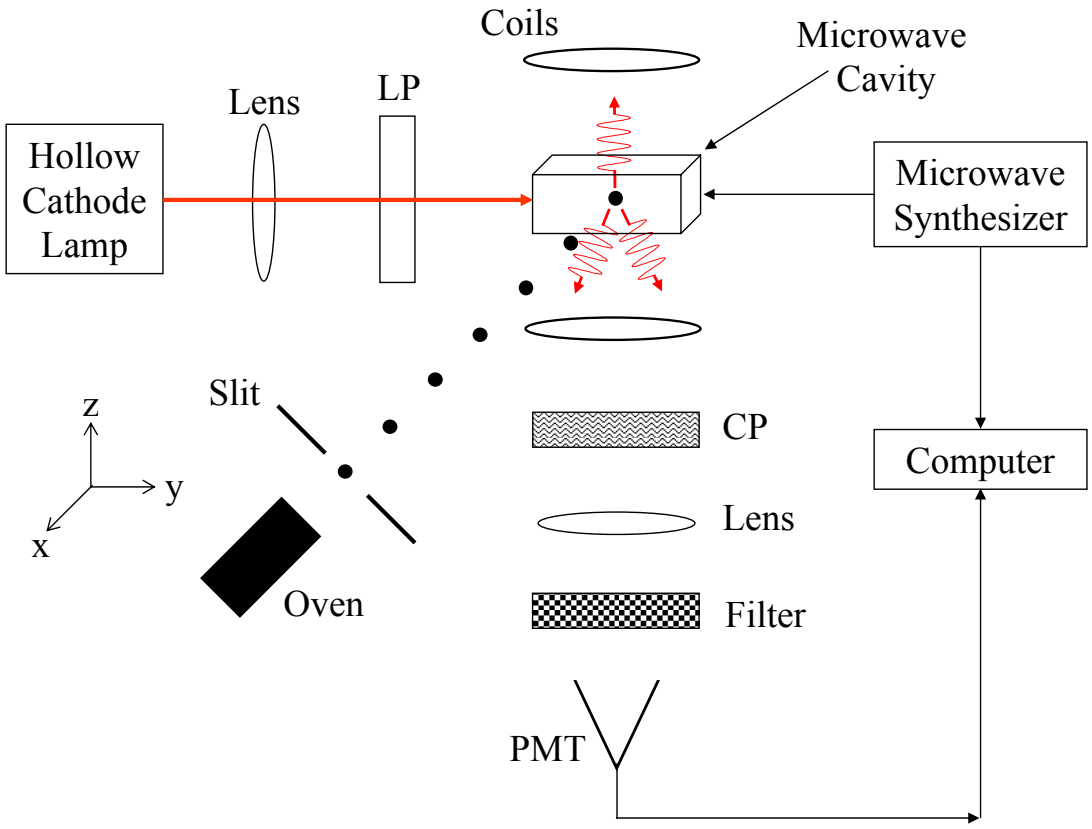

Figure 2.4: Apparatus for Optical Double Resonance Experiment used by Orth et al

The apparatus used by Orth et al is illustrated in Fig. 2.4. An atomic beam was generated using an oven similar to that described in the previous section. The atoms traversed in the -x direction and passed through a microwave cavity. At the center of the microwave cavity, the atoms were excited by resonant light generated by a hollow cathode lamp. This light passed through a linear polarizer (LP) and was directed

along the y axis. Two pairs of Helmholtz coils were used to generate a magnetic field in the z direction of up to several hundred Gauss uniform to about 100 ppm in the microwave cavity. A microwave synthesizer generated nearly 20 W of power at the fixed frequency 9,580.000 MHz. Fluorescence emitted in the -z direction was detected by a photomultiplier (PMT). The fluorescence passed through a circular polarizer (CP) and an interference filter which reduced the detection of scattered background light. The photomultiplier signal was detected as a function of the magnetic field which was varied in 5 G increments. The field strength was determined using a Rb magnetometer. A value of 10,053.184 $\pm$ 0.058 MHz was obtained for the ^{7}Li 2P fine structure interval by fitting this signal.

2.2.3 Frequency Modulation

The ^{6,7}Li isotope shifts of the D1 and D2 lines have been found using Doppler free frequency modulation spectroscopy (FM) [14]. This technique, developed by Bjorklund et al, basically is a saturation spectroscopy experiment using two counter-propagating laser beams that travel through an atomic vapour [37, 38]. One laser beam called the "pump" laser alters the population of the atomic levels which is then measured by the second weaker "probe" laser.

The apparatus used in this experiment is shown schematically in Fig. 2.5. A saturated absorption signal was obtained using a weakly collimated atomic beam and a ring dye laser. The dye laser generated 250 mW of power at a wavelength

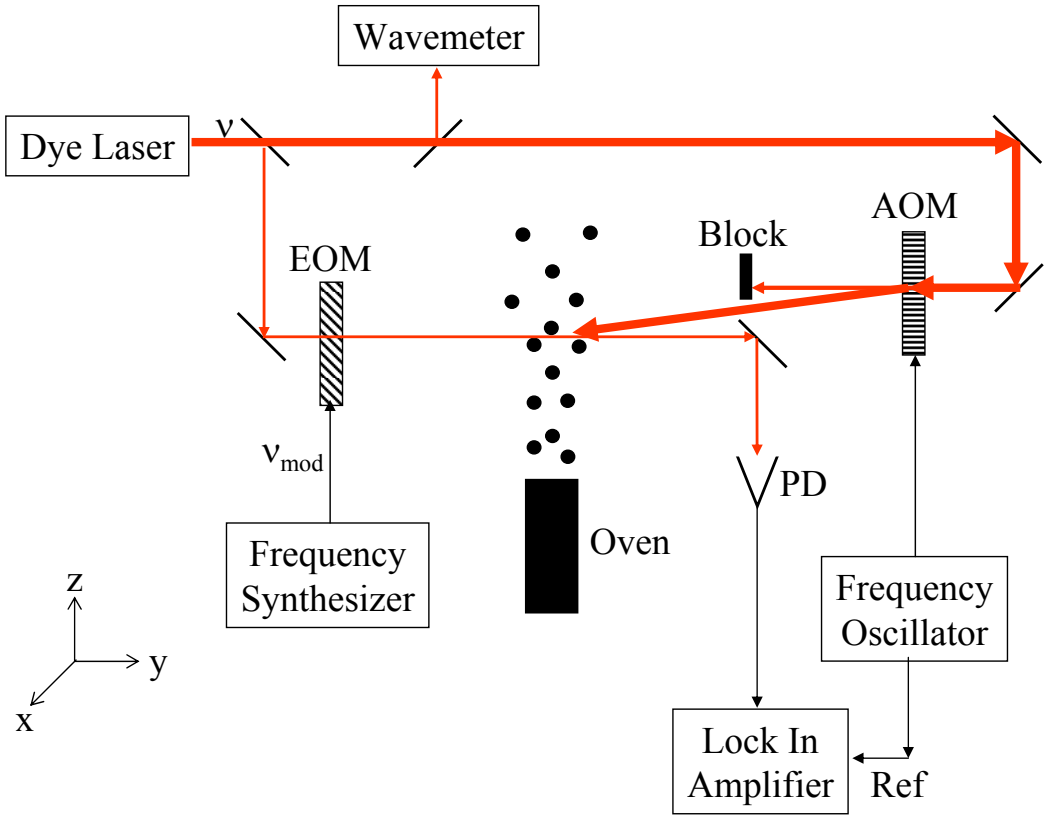

Figure 2.5: Apparatus of Frequency Modulation Experiment used by Sansonetti et al

of 670.1 nm with a linewidth of about 1 MHz. Part of the laser beam was directed into a wavemeter to measure the absolute laser frequency to a few parts in 10^9. A Fabry Perot marker etalon not shown in Fig. 2.5 monitored the laser frequency as it was scanned. The remainder of the laser beam was split into pump and probe beams that counter-propagated through the lithium vapour cell. The pump laser beam passed through an acousto-optic modulator (AOM) which acts as an optical isolator preventing reflection of laser light back into the dye laser. The acousto-optic

modulation frequency of 72 MHz was itself chopped at 80 kHz. The probe laser beam passed through an electro-optic modulator (EOM) creating sidebands containing 10% of the laser power at $\nu_{mod} = 20$ MHz intervals around the central laser frequency. The sidebands probed the saturated absorption induced by the pump beam as the dye laser was scanned across a lithium resonance. The probe laser beam was attenuated when its frequency coincided with a lithium resonance. Part of the probe laser beam was focussed onto a fast photodiode (PD). This signal was then sent to a lock in amplifier whose reference was supplied by the 80 kHz chopping frequency sent to the AOM.

Absolute transition frequencies of the D1 and D2 lines were found using the fine and hyperfine splittings of the 2P states found in previous experiments [7] and [12]. The 2P hyperfine splittings could not be completely resolved and caused the signals to be asymmetric. The isotope shifts of the D1 and D2 transitions were determined to be $10,532.9 \pm 0.6$ and $10,533.3 \pm 0.5$ MHz, respectively.

2.2.4 Laser Atomic Beam

Several groups have done experiments using a laser to excite a collimated atomic beam (LAB) [8–10, 13]. This generates much narrower spectral lines which are limited by the transition natural linewidth instead of the much larger Doppler width observed in a cell. Typically, fluorescence is observed while the laser frequency is scanned across the resonance. This enables one to determine the fine structure interval, isotope shift and the hyperfine splittings of the lower and excited states.

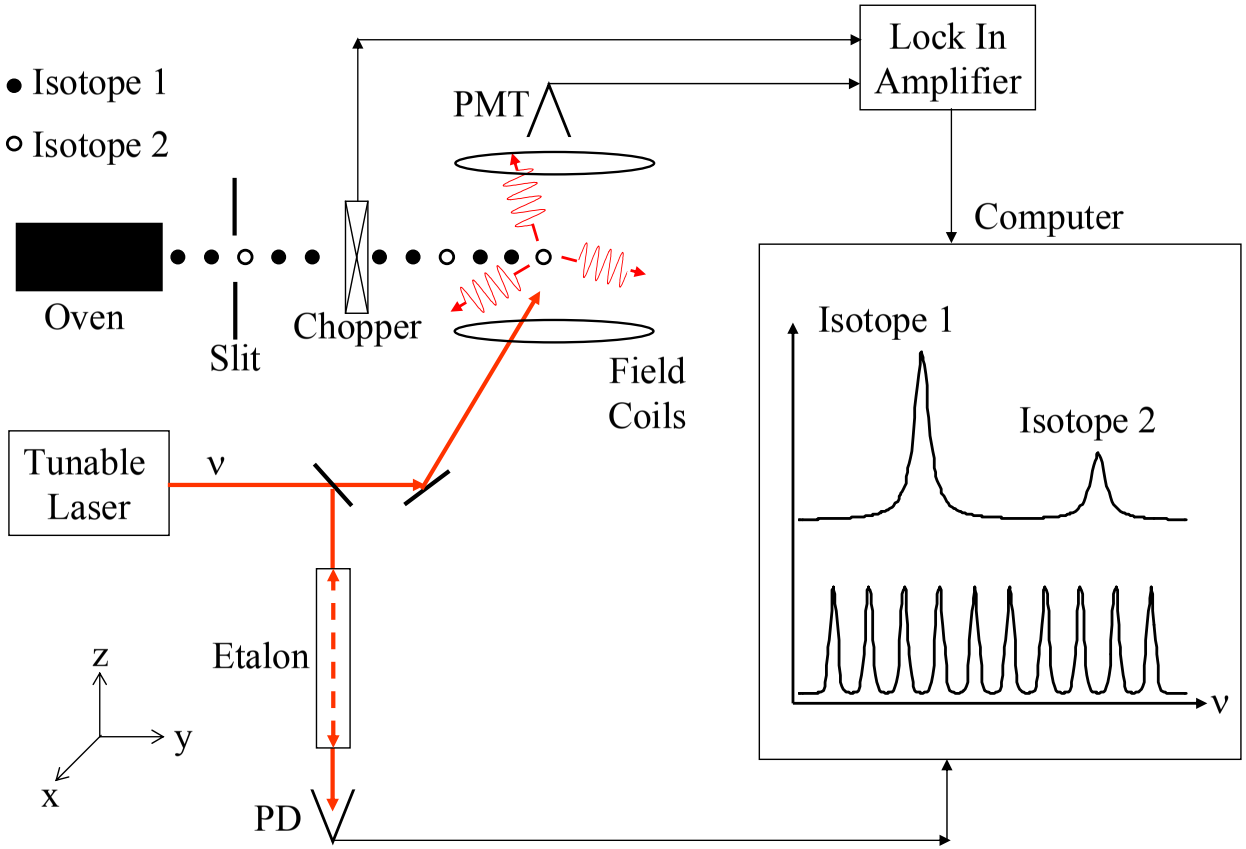

Figure 2.6: Laser Atomic Beam Apparatus used by Windholz et al

The group of Windholz et al has made several studies of the Li D lines using the apparatus illustrated in Fig. 2.6 [8, 9, 13]. The atomic beam was generated by heating lithium in an oven and collimating the atoms with a slit. The resulting beam had a divergence of about 1 milliradian. The atomic beam also passed through a mechanical chopper. A cw dye laser beam having a linewidth of about 3 MHz intersected the atomic beam orthogonally to minimize Doppler broadening. Some of the experiments used a magnetic field of up to 100 G that was generated using Helmholtz coils. Fluorescence was detected as the laser frequency was scanned across the resonance. The change in laser frequency was determined by passing part of the laser beam through a high finesse etalon. A transmission peak occurred whenever the laser frequency changes by an amount equal to the cavity free spectral range which is inversely proportional to the etalon length.

A critical step in these experiments was the calibration of the etalon. This is typically done using a reference HeNe laser whose frequency was locked using an iodine reference cell. The etalon is normally isolated in a vacuum chamber to minimize vibrations as well as fluctuations in temperature and pressure. Unfortunately, a number of groups have had difficulties in determining the etalon free spectral range. The Windholz group repeated their experiment three times to resolve conflicting results for the D2 isotope shift and the 2P fine structure interval.

A recent laser atomic beam experiment was performed by the group of Das et al using a home built diode laser [10]. Their apparatus is illustrated in Fig. 2.7.

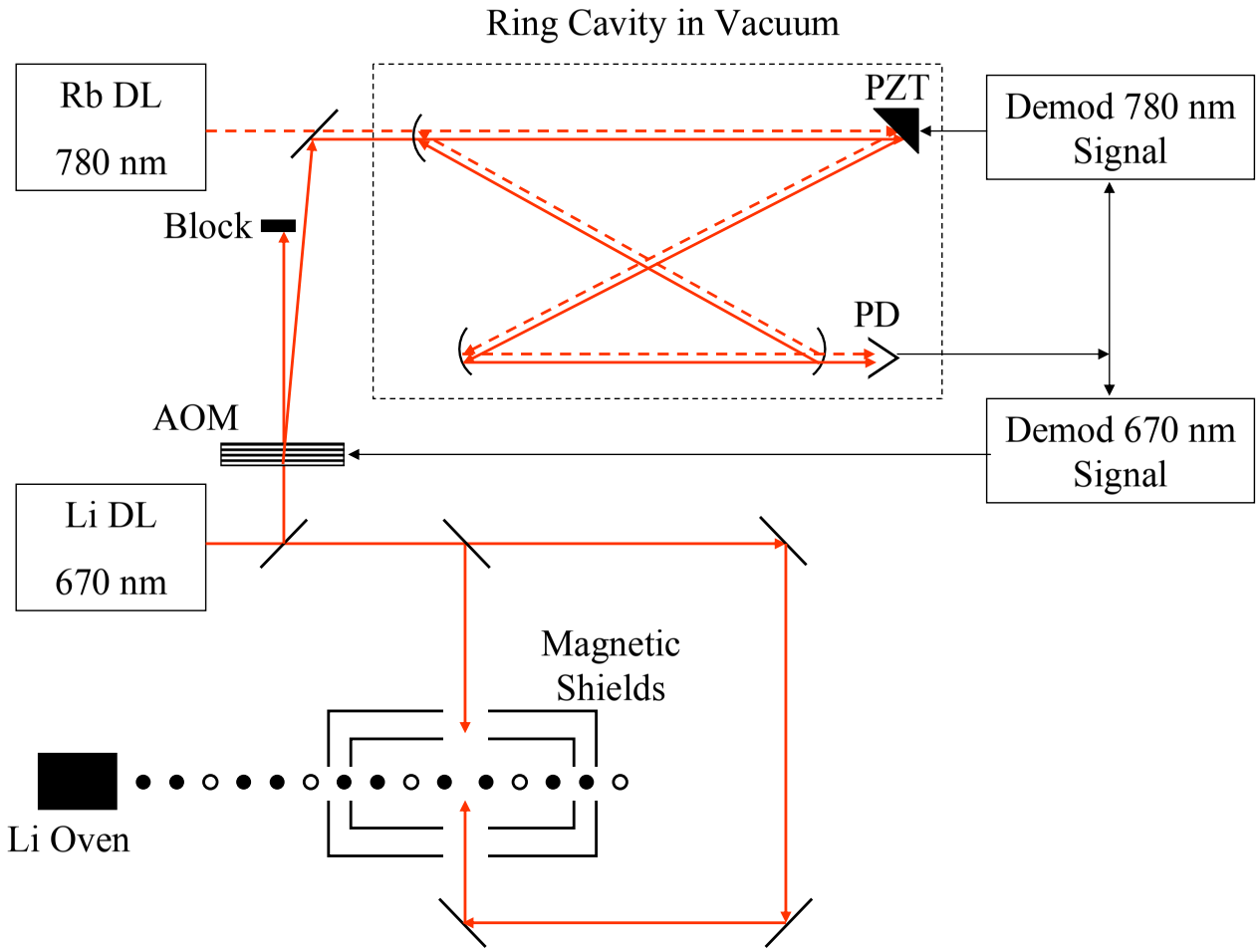

Figure 2.7: Laser Atomic Beam Apparatus used by Das et al

The laser operating at 670 nm (Li DL), was locked to the lithium resonance and absolute transition frequencies of the ^{6,7}Li D lines were determined. This was done by frequency shifting part of the diode laser beam by an AOM. The resulting laser beam was directed into an optical cavity whose length could be tuned by varying the position of one mirror mounted on a piezoelectric transducer (PZT). The cavity length was stabilized using another diode laser (Rb DL) that was locked to one of the hyperfine transitions of the D2 line of ^{87}Rb at 780 nm. The unknown diode laser frequency was found by measuring the AOM frequency required for the laser to be in resonance with the cavity and using the known wavelength of the Rb transition.

The experimental results of the D1 and D2 isotope shifts and the 2P fine structure list an uncertainty of about 50 kHz. Unfortunately, this analysis was done using an incorrect value for the electric quadrupole hyperfine constant of the ^{6}Li $2P_{3/2}$ state [39]. The same apparatus has also been used to measure the hyperfine splitting of the ^{7}Li $2P_{1/2}$ state [40]. The resulting magnetic dipole constant disagrees by 9σ from those found by other experimental and theoretical groups [41].

2.2.5 Laser Atomic Beam using electro-optic modulation

The problems associated with accurate etalon calibration can be avoided using a laser beam modulated using either an acousto or electro-optic modulator [42], [43], [44]. The laser frequency is scanned across the resonance while fluorescence produced from the decay of the excited state is detected. Each atomic transition generates

multiple peaks separated by the modulation frequency. The latter is conveniently specified to high accuracy by a frequency synthesizer. Hence, each laser scan is calibrated. One can also check for any scan nonlinearity by passing part of the laser beam through an etalon.

The apparatus used to apply this technique to study the Li D lines is shown in Fig. 2.8 [11]. An atomic beam directed in the y direction was generated by heating a sample of lithium metal to several hundred degrees centigrade. The lithium atoms were excited using a diode laser that produced a laser beam having a power of 12 mW at 670 nm. The laser was frequency modulated using either a 6.8 or 9.2 GHz electro-optic modulator. The modulation frequency was specified by a frequency synthesizer and chosen such that the various fluorescent peaks did not overlap. The laser beam was linearly polarized along the z direction, perpendicular to the atomic beam.

The laser frequency could be scanned up to 15 GHz by adjusting a grating. The scan linearity was monitored by passing part of the laser beam through a confocal etalon having free spectral range of nearly 300 MHz. The etalon was constructed using an invar rod to minimize temperature variation effects. A photodiode (PD) monitored the laser beam transmitted through the etalon. Fluorescence emitted in the z direction was detected by a photomultiplier (PMT). A single laser scan generated a data file having 10,000 points where each point represented about 1 MHz.

A sample signal is shown in Fig. 2.9. This figure shows the nonlinearity of the laser scan which was taken into account in the data analysis. The results were

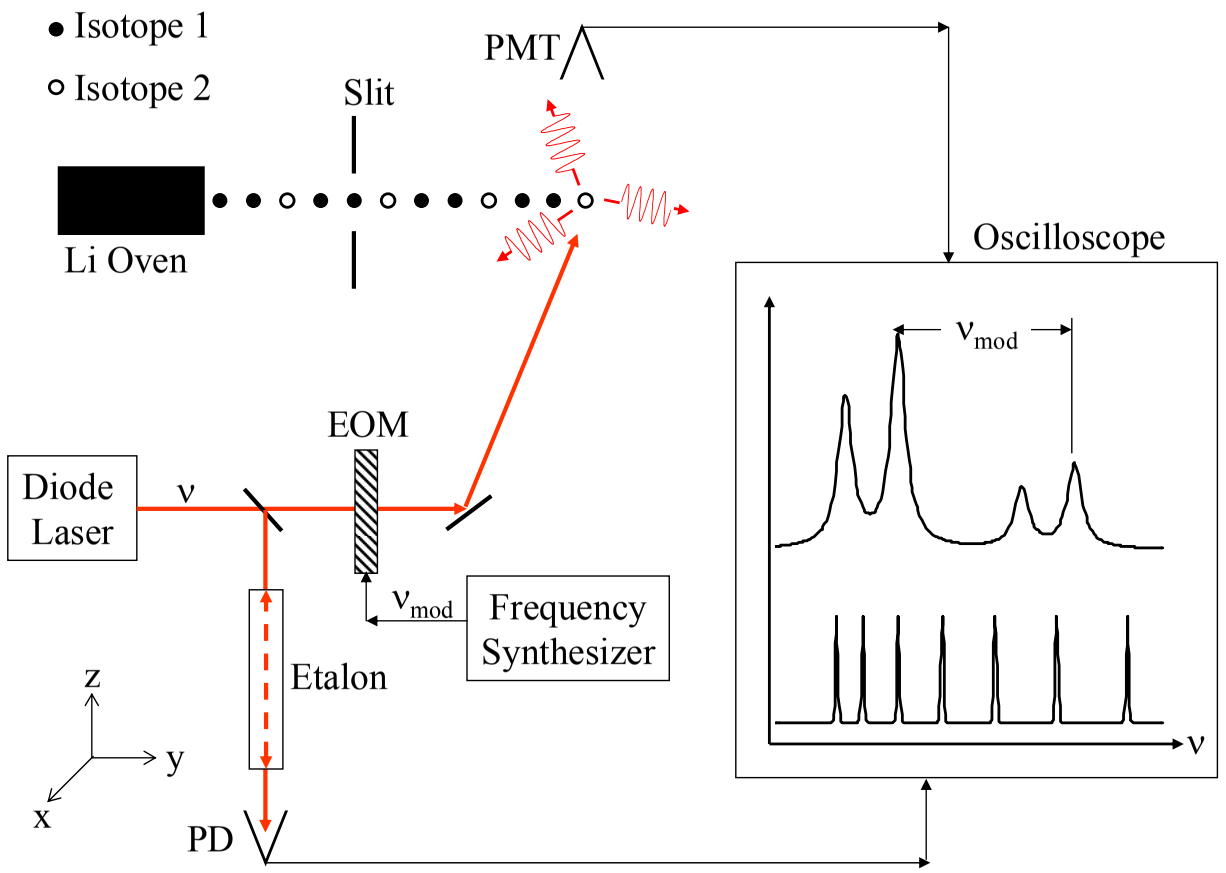

Figure 2.8: Laser Atomic Beam Excitation with Electro-Optic Modulation used by Walls et al

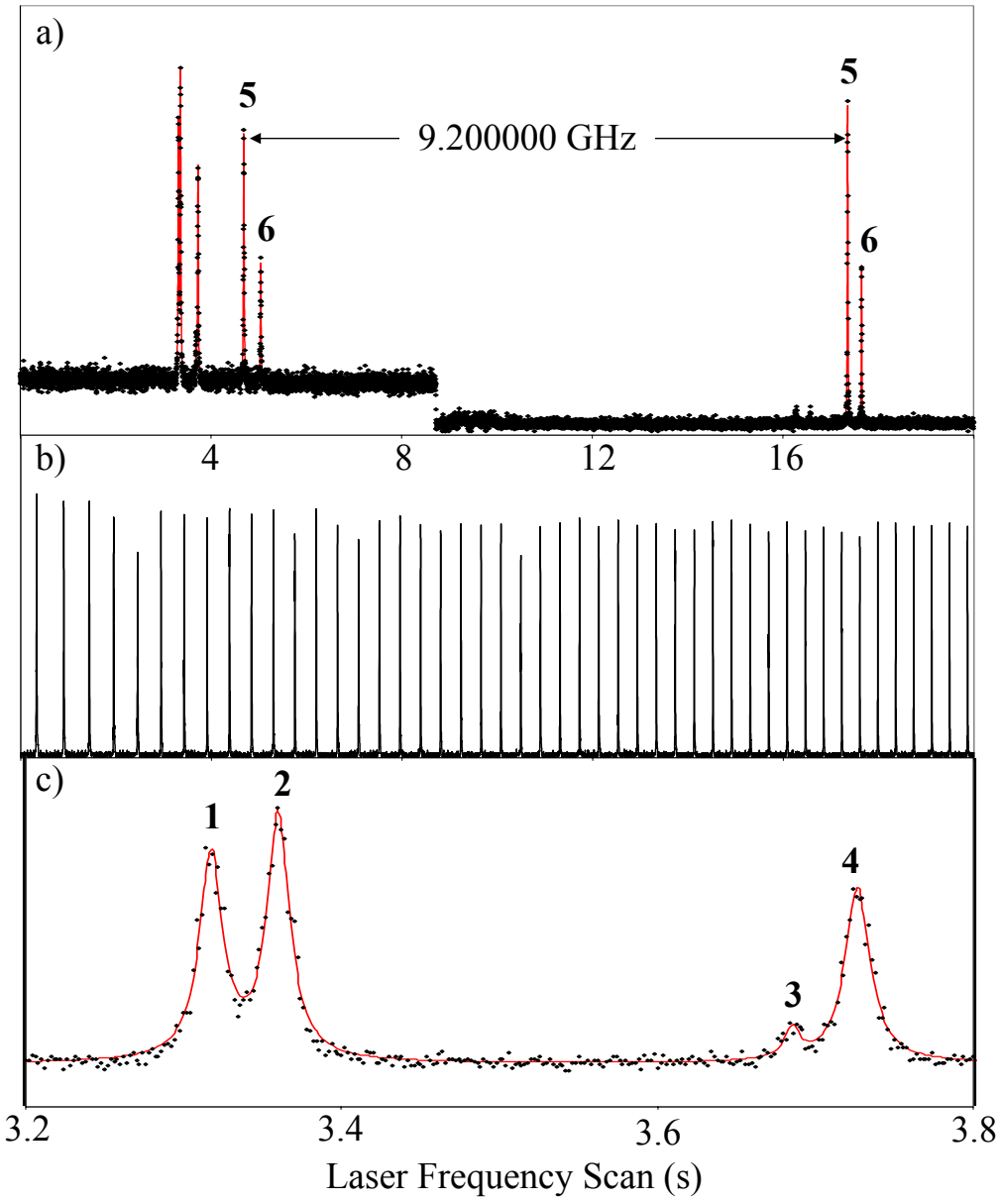

Figure 2.9: Sample ^{6}Li Laser Scan by Walls et al. Figure (**a**) shows the fluorescence (black dots) taken during a laser frequency scan along with the fitted spectrum. Each transition was excited twice due to electro-optically modulating the laser frequency at 9.2 GHz. A neutral density filter was inserted midway during the scan to avoid saturating the photomultiplier by the D2 line. Figure (**b**) shows the transmission of part of the laser beam through an etalon. The first two peaks shown in (**a**) were the ^{6}Li D1 lines and were actually the 4 peaks as shown in (**c**).

tested by checking that the ^{6,7}Li ground state hyperfine splittings agreed with the results of atomic clock experiments [45]. The resolution of about 1 MHz per point was insufficient to resolve the relative contributions of the various $2P_{3/2}$ hyperfine levels to the fluorescence peaks. A model to account for optical pumping effects was therefore used to fix the relative contributions of the excited state hyperfine levels to the observed signals when fitting the data.

2.3 Li 2 $^2S_{1/2} \rightarrow 3\ ^2S_{1/2}$ Transition

The two photon $2\ ^2S_{1/2} \rightarrow 3\ ^2S_{1/2}$ transition was studied using Doppler free spectroscopy. The apparatus, illustrated in Fig. 2.10, was developed at the GSI accelerator to first study the stable isotopes ^{6,7}Li [15] and subsequently the radioactive isotopes ^{8,9}Li [16]. It was later moved to the TRIUMF accelerator which generated a high flux of ^{11}Li [17]. All the experiments were done in a weakly collimated atomic beam.

The two photon transition $2\ ^2S_{1/2} \rightarrow 3\ ^2S_{1/2}$ was excited using light produced by a titanium sapphire (TIS) ring laser operating at 735 nm. The upper $3S_{1/2}$ state was then ionized using another laser beam. The ions were separated and detected using a quadrupole mass spectrometer. The ion signal was measured as a function of the TIS laser frequency with a resolution of approximately 1 MHz per channel. The resulting signal peaks were fitted using two Gaussian pedestals corresponding to

Doppler broadened excitation of the background gas and the atomic beam as well as a Voigt profile that described the Doppler free excitation. Each experiment was tested by measuring the magnetic dipole hyperfine constant of the Li $3S_{1/2}$ state and the $2S \rightarrow 3S$ transition energy. The results of these quantities agreed with theory as well as previous measurements but were an order of magnitude more accurate.

The initial experiment used a TIS laser that was frequency stabilized and scanned by offset locking to a single mode HeNe laser using an evacuated and temperature stabilized confocal interferometer [15]. The latter was calibrated using the ^{87}Rb ground state hyperfine splitting observed in the $5S \rightarrow 5D$ two photon excitation at 778 nm. The Li $3S_{1/2}$ state was ionized using an Ar^+ laser operating at 514 nm. The isotope shift for the transition has a 30 kHz error that appears to be dominated by statistical uncertainty.

The experiment was refined to enhance the efficiency of ion detection to enable the study of the radioactive isotopes as well as ^{6,7}Li [16]. The TIS laser first excited the $2S \rightarrow 3S$ two photon transition. The upper state spontaneously decays to the $2P_{1/2,3/2}$ states. A dye laser operating at 610 nm then excited the $2P_{3/2} \rightarrow 3D_{3/2,5/2}$ transition. This state was subsequently ionized by either the dye or TIS laser photons. Laser intensities of ≈ 17 W/mm^2 were required to saturate the transitions. These intensities were attained by enclosing the interaction region of the lasers with the lithium atoms in an optical cavity. This enhanced the laser power by a factor of 100. The resonator was locked to the TIS laser while the dye laser was locked to the

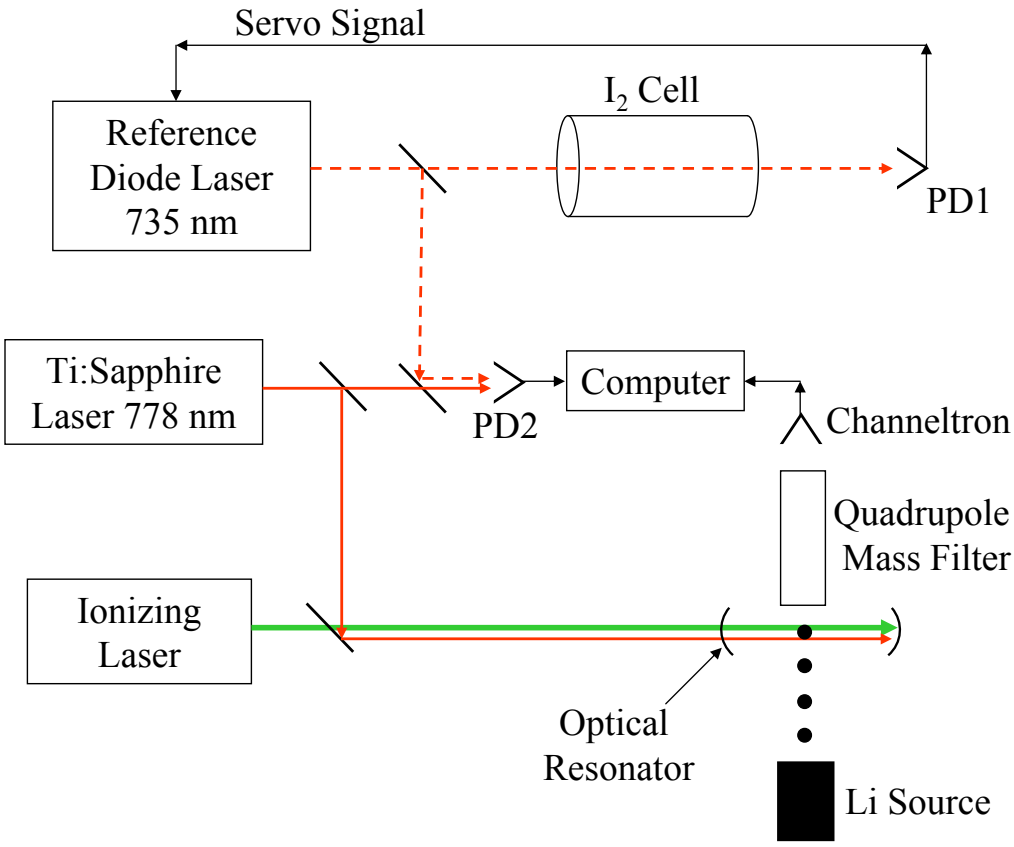

Figure 2.10: Apparatus for studying the 2 $^3S_{1/2} \rightarrow 3\ ^2S_{1/2}$ transition used by Sánchez et al

resonator. Efficient excitation occurred even though the dye laser was not tuned to the center frequency of the transition because the resonance was power broadened. The TIS laser was stabilized by frequency offset locking to a reference diode laser that was in turn locked to an iodine line using photodiode PD1. A photodiode PD2 having a 25 GHz bandwidth detected the beat frequency between the TIS and diode lasers. An important systematic effect was that the beat frequency shifted as a function of the TIS laser power. Data were therefore taken at a variety of laser powers. The isotope shift, extrapolated to zero power has an uncertainty of 130 kHz which is dominated by this ac Stark shift correction.

The most recent isotope shift measurement was obtained at the TRIUMF accelerator [17]. It has an uncertainty of only 20 kHz which is over six times smaller than that of their previous experiment [16]. No reason is given for this. Their latest result disagrees with their initial experiment by about 5 times the combined uncertainties. This discrepancy is attributed by the authors to unaccounted systematic error in the interferometric measurements of the original work.

3 Apparatus

This experiment determined the isotope shifts of the D1 and D2 lines as well as the fine structure interval of the 2P states by using an electro-optically modulated laser beam to excite a neutral atomic beam. This spectroscopic technique was developed in our group about ten years ago [46]. The apparatus is illustrated in Fig. 3.1. This chapter describes the various components.

3.1 Vacuum System

A vacuum was used to generate an atomic beam. The system consisted of two chambers, one that contained the oven and a second where the laser and atomic beam intersected. The two chambers were each pumped by an Edwards diffusion pump (Diffstak 160) which has a pumping speed of 700 liters/sec [47]. Each diffusion pump was in turn backed up by a Edwards rotary pump (RV8) which had a pumping speed of 3 liters/sec [48]. The pressure was monitored using an ion gauge (Granville-Philips Model 274003). A pressure of 1.0×10^{-7} Torr was achieved after about 12 hours of continuous pumping.

3.2 Magnetic Field Nulling Coils

The magnetic field in the region where the laser intersected the atomic beam was nulled to reduce Zeeman broadening of the spectral lines which could reduce the

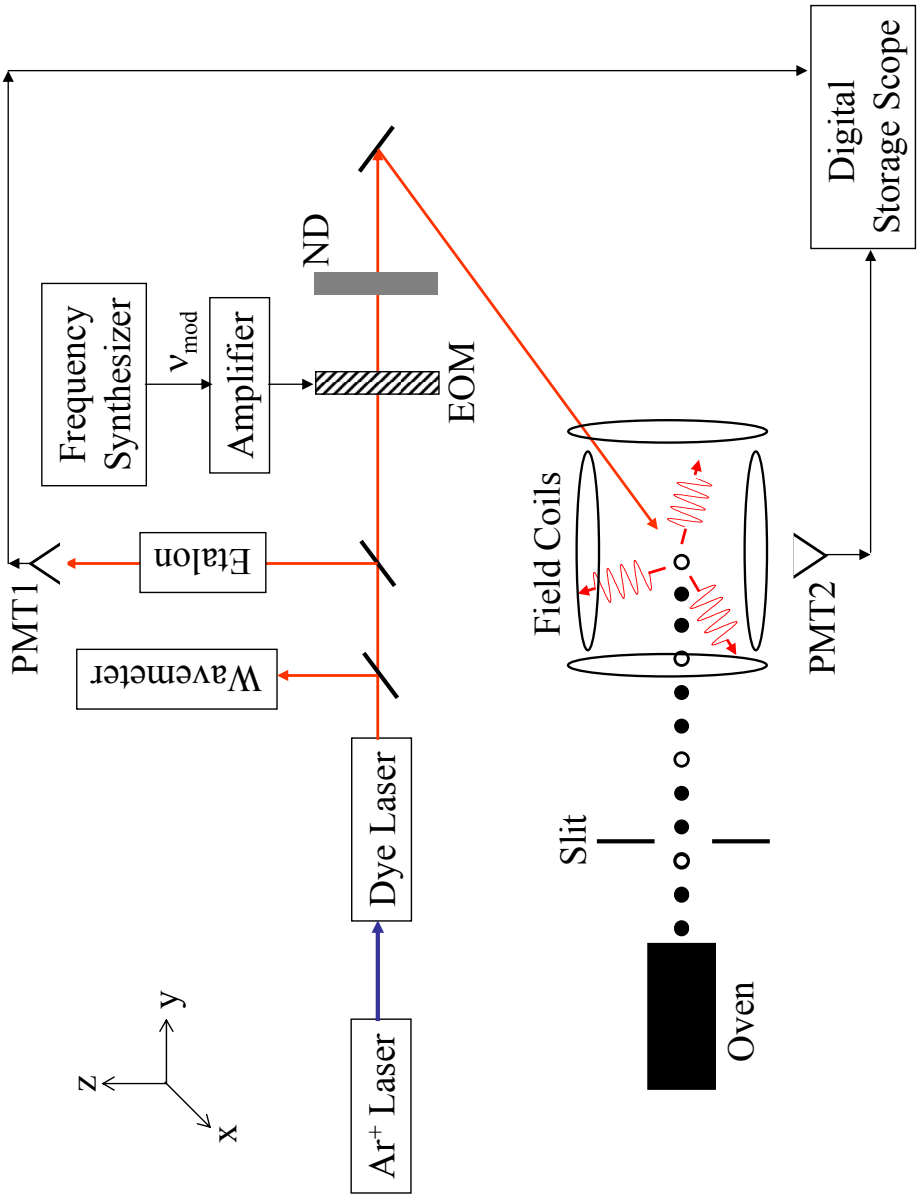

Figure 3.1: Apparatus

resolution. Three pairs of coils aligned along the x, y and z axes (two pairs of coils are shown shown in Fig. 3.1) were used to cancel the Earth's magnetic field. The coils were created by wrapping copper wire having a diameter of 1.3 mm around the vacuum chamber. The x, y and z coils contained 25, 50 and 25 windings and the currents required to null the magnetic field at the coil centers were 40, 65 and 200 mA, respectively. These currents were adjusted by monitoring the magnetic field using a Hall Effect Gaussmeter (F. W. Bell 620 Gaussmeter). The residual magnetic field was less than 20 mG and was found to remain stable when checked periodically between runs.

3.3 Lithium Oven and Atomic Beam Generation

A neutral beam of lithium atoms was created by first heating lithium metal in an oven. The emitted atoms were then collimated using a series of narrow slits. This enabled the first order Doppler shift to be negligible when the laser intersected the atomic beam orthogonally. The oven is illustrated in Fig. 3.2. It was loaded with lithium metal that was commercially available from Sigma Aldrich. The lithium metal was shipped immersed in a can of mineral oil to minimize oxidation. The oil was wiped off and about 10 g was loaded into the oven. Both natural lithium and pure ^{6}Li samples were used in the experiment.

The oven was heated to about 400 °C which was monitored using an Omega Type

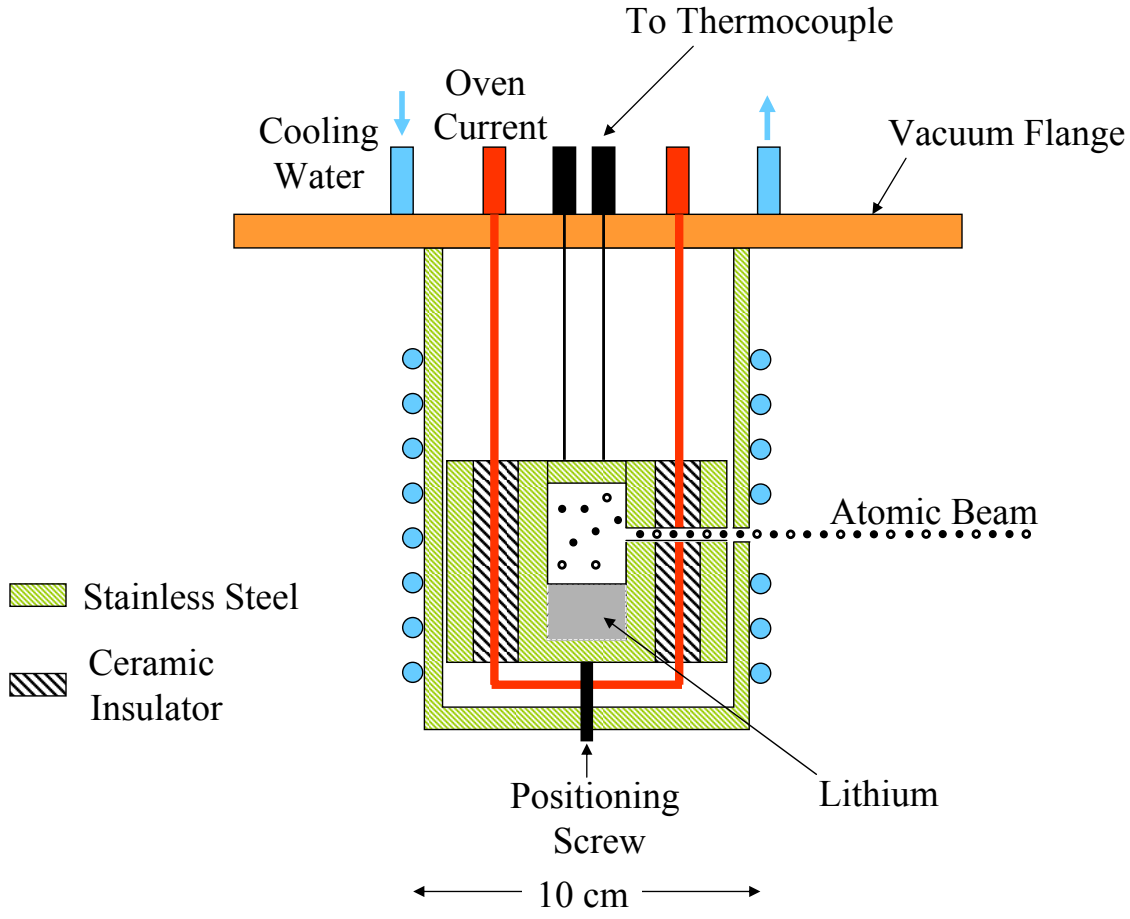

Figure 3.2: Lithium Oven

K thermocouple (Ni-Cr and Ni-Al). For reference, the melting point of lithium is 180 °C while the boiling point is 1350 °C. The oven was heated by applying a 20 V AC current through a 100 cm length of tungsten wire having a diameter of of 0.05 cm. The wire was insulated by hollow ceramic spacers from the stainless steel oven walls. The outside of the oven in contact with the vacuum flange was water cooled to maintain the integrity of the O-ring seal.

Atoms were emitted from the oven through a small hole. The atoms were further collimated using a series of narrow slits to generate the atomic beam. The resulting beam had a divergence of $\leq$ 2 milliradians. The atomic beam flux is believed to be comparable to that of a barium source that generated about approximately 10^9 atoms/sec [49]. That neutral atom flux was measured using a so called hot wire detector. The barium atoms struck a hot tungsten filament that ionized the atoms. An ammeter measured the resulting ion current. Each load of lithium metal could produce an atomic beam for a duration of up to 20 hours.

3.4 Coherent 699 Ring Dye Laser

Laser light resonant with the lithium D1 and D2 transition wavelength of 670 nm was generated using a ring dye laser (Coherent 699) [50]. The laser frequency was measured by a wavemeter (Burleigh WA-1500) which had an accuracy of $\pm$ 0.2 ppm. The dye laser was pumped by an Argon Ion laser (Coherent Innova 200) that generated 5 W of power at 514 nm. The laser dye was prepared by first dissolving 1 g of DCM (Exciton) in 400 mL of benzyl alcohol. This was inserted into an ultrasonic cleaner for up to half an hour to facilitate fully dissolving the dye. The solution was then poured into 600 mL of ethylene glycol and then into the dye circulator.

The dye laser generated a beam having a power of about 400 mW with a TEM_{oo} mode. The laser was linearly polarized along the vertical direction. The laser fre-

quency could be scanned without mode hops for up to nearly 36 GHz at the slowest speed of about 60 MHz/sec by rotating a small glass plate which varied the optical length of the laser cavity. The manufacturer quoted laser linewidth is 0.5 MHz [50]. The laser beam diameter was about 2 mm. The power was measured to be 1 mW before the laser entered the vacuum chamber. This yielded an intensity of 0.3 mW/mm^2 which is more than an order of magnitude less than the saturation intensity of 5.1 mW/mm^2 [51].

Special care was taken to ensure stable operation of the dye laser. It was enclosed in a plastic box to minimize dust accumulation and an air filter (Laminaire LP24) removed dust particles. Vibrations were minimized by mounting the Ar^+ and dye lasers on a 20 cm thick optical table (Newport Technical Series Model MST-410-8). This was levitated on a nitrogen cushion. The laser was run for up to 12 hours for a single set of data collection runs. Afterwards, the dye was changed.

3.5 Fabry Perot Etalon

Part of the dye laser beam was directed into a Fabry Perot Etalon (Burleigh CFT-500) to monitor the linearity of the dye laser frequency scan as shown in Fig. 3.1. This etalon consisted of two mirrors each having a reflectivity of >99% at 670 nm, mounted on an invar rod having a length L. The interferometer length was very stable as invar has a low temperature coefficient of expansion. The etalon was arranged in

the confocal geometry meaning that the mirror radius of curvature equals the cavity length. Hence, the round trip distance for a light beam is approximately 4L.

The transmission of the laser through the etalon was monitored by a photomultiplier (PMT1). A transmission peak occurs every free spectral range given by $FSR = c/4n\mathrm{L}$, where n is the index of refraction of the air inside the cavity and c is the speed of light in vacuum. The resulting signal was recorded by a digital oscilloscope (Tektronix TDS 5054 B). The calibration of the free spectral range is described in section 4.1.

3.6 Electro-Optic Modulator

The dye laser frequency was frequency modulated using an electro-optic modulator (EOM) as shown in Fig. 3.1. Two modulators operating at 6.8 and 9.2 GHz (New Focus 4851M and 4851) were used. The EOM consisted of a MgO doped $LiNbO_3$ crystal. The crystal was antireflection coated for 500-900 nm light. The crystal was housed in a microwave cavity tuned to be resonant with the modulation frequency [52].

The modulation frequency was generated by a microwave synthesizer (Agilent E8241A) which had an accuracy to 3 parts in 10^7 [53]. The synthesizer signal had a power of 6.3 mW and was input to a water cooled amplifier (Quinstar QPN-08403534) by a 50 cm SMA cable. The signal coming out of the amplifier had a power of 3 W.

It was carried through a 20 cm SMA cable to the EOM.

The EOM added frequency sidebands to the incident laser beam which had a frequency ν such that the output laser beam had frequency components $\nu \pm n\nu_{mod}$ where n is an integer. All of the sidebands have the same linear polarization and are collinear with the unshifted laser frequency beam component. About 20% of the incoming laser power was transferred into the sidebands at frequencies $\nu \pm \nu_{mod}$ [54].

3.7 Fluorescence Detection System

The electro-optically modulated laser beam was directed into the vacuum chamber using a pair of slits mounted on either side of the vacuum viewports as shown in Fig. 3.1. This was done to ensure that the laser beam intersected the atomic beam orthogonally to eliminate the first order Doppler shift. The laser was linearly polarized along the z direction. The laser power was varied by a factor of two using neutral density filters (ND).

Fluorescence, produced by the laser excitation of the atomic beam and subsequent radiative decay of the excited lithium 2P state, was detected by a photomultiplier (PMT2) (Hamamatsu R928). The photomultiplier had a quantum efficiency of 7% at 670 nm. The latter efficiency refers to the number of photoelectrons emitted from the photomultiplier's photocathode per second divided by the number of incident photons per second. The photomultiplier was mounted along the z axis to minimize

its detection of scattered laser light. The photomultiplier voltage was set between 400 and 500 V. This voltage was chosen to avoid saturating the signal which was tested using a neutral density filter that attenuated the light by 50%.

The two signals from the two photomultipliers were collected by a digital oscilloscope (Tektronix TDS 5054 B). Data were recorded at a rate of 4000 Hz during the entire 15 GHz laser scan. Each scan took about 5 minutes resulting in a data file consisting of over one million points. Each data point was saved with a resolution of 8 bits [55]. Up to 100 runs were taken on any given day. These files were transferred to a pentium computer (Dell Optiplex GX270) for analysis.

4 Data Analysis

This chapter discusses first how the positions of the Fabry Perot transmission peaks were found. This information is critical to determine the linearity of the laser frequency scan. Next, the fitting of the fluorescence peaks is presented. This is followed by a determination of the hyperfine splittings of the ^{6,7}Li ground state and $2P_{1/2}$ excited state which stringently test the measurement technique.

4.1 Linearity of Laser Frequency Scan

Each laser scan produced a file containing the laser intensity transmitted through the Fabry Perot etalon versus time as shown in Fig. 4.1. The Fabry Perot peak centers were determined by averaging the times on the left and right of the peak where the laser transmitted intensity was half of the peak intensity. This was done using a computer program discussed in Appendix A.

It is critical to check the linearity of the laser scan to accurately determine the positions of fluorescence peaks occurring between Fabry Perot peak markers. The scan linearity was examined by plotting the times at which the 245 peak centers occurred as shown in Fig. 4.2. These data were taken using a ten times faster scan speed than used to collect fluorescence data because the oscilloscope had insufficient memory to record a slower scan encompassing 36 GHz. The scan nonlinearity was observed to be about double at this speed than at the slower scan rate.

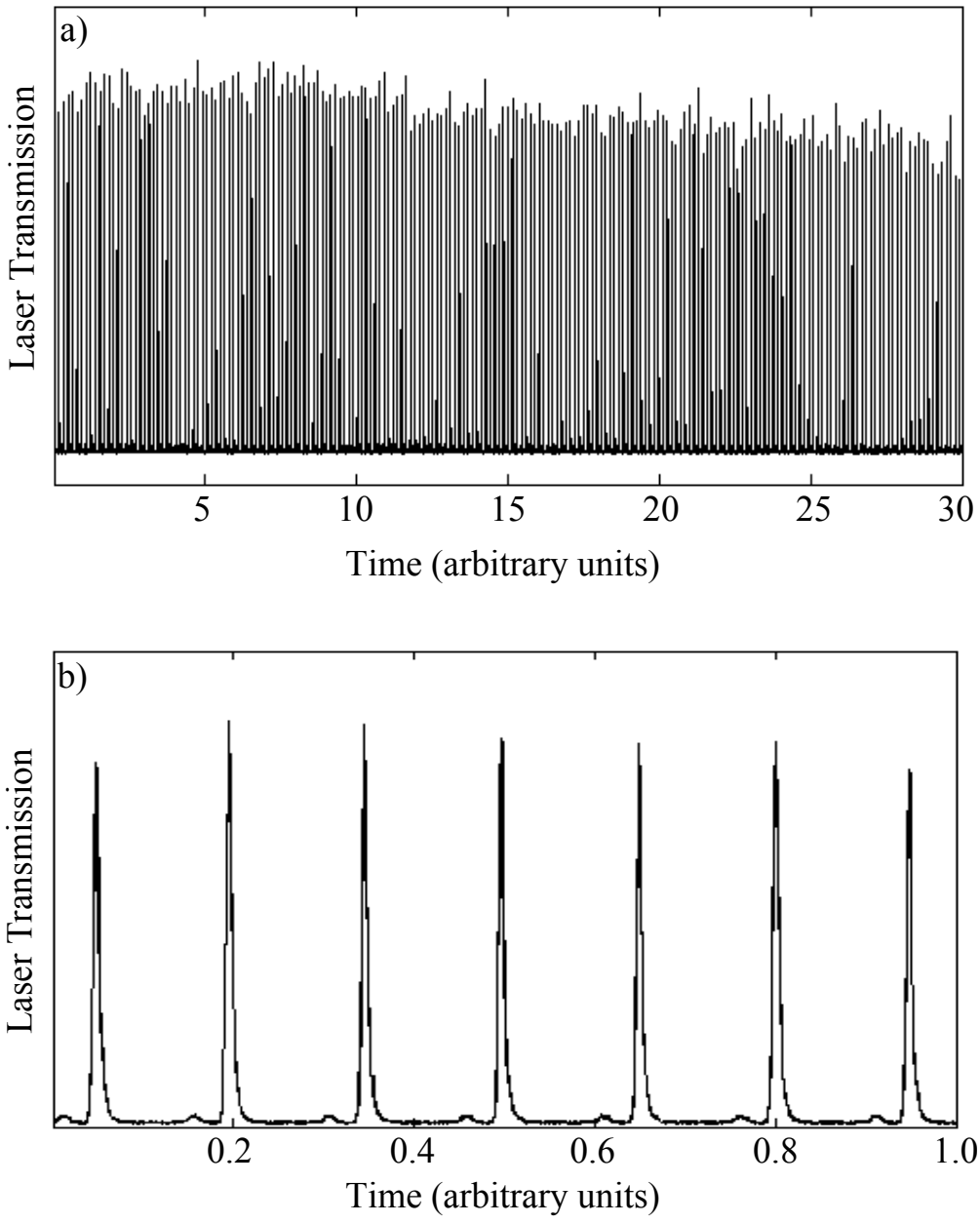

Figure 4.1: Laser Transmission Through Fabry Perot Etalon during (**a**) full laser scan and (**b**) section of the laser scan.

The linearity of the laser scan was checked by fitting a polynomial of degree n to the data and plotting the difference between the data and the fitted curve as shown in Fig. 4.3. A linear fit to the data gave an average time between peaks of 0.151 sec. This linear coefficient increased to 0.155 and 0.158 sec when polynomials of degree 3 and 5 were fitted, respectively. The nonlinear terms therefore change the linear scan rate coefficient by a maximum of 4.6% during a full scan encompassing 245 Fabry Perot peaks. Hence, the effect of this nonlinearity over a single free spectral range interval is only 0.019%.

In this experiment, the frequency intervals separating two fluorescent peaks were measured. Each fluorescent peak position was determined relative to the nearest Fabry Perot marker peak. This frequency interval was less than half of one free spectral range (FSR). Hence, the maximum effect of the laser scan nonlinearity on this peak position is 0.019% $\times$ 0.5 $\times$ FSR. For a FSR of approximately 150 MHz, this equals 14 kHz. A frequency interval was found by subtracting two fluorescent peak positions. The maximum uncertainty was given by adding the uncertainties of the two peak positions in quadrature to give 20 kHz.

This experiment further reduced the effect of the laser scan nonlinearity by estimating the position of each fluorescent peak using the nearest 6 Fabry Perot peaks (3 on either side) and fitting a polynomial of degree 5 to the frequency scan. Fig. 4.3 shows the average root mean square of the residuals was reduced by nearly an order of magnitude when the fitting polynomial degree is 5 as compared to a degree of 1.

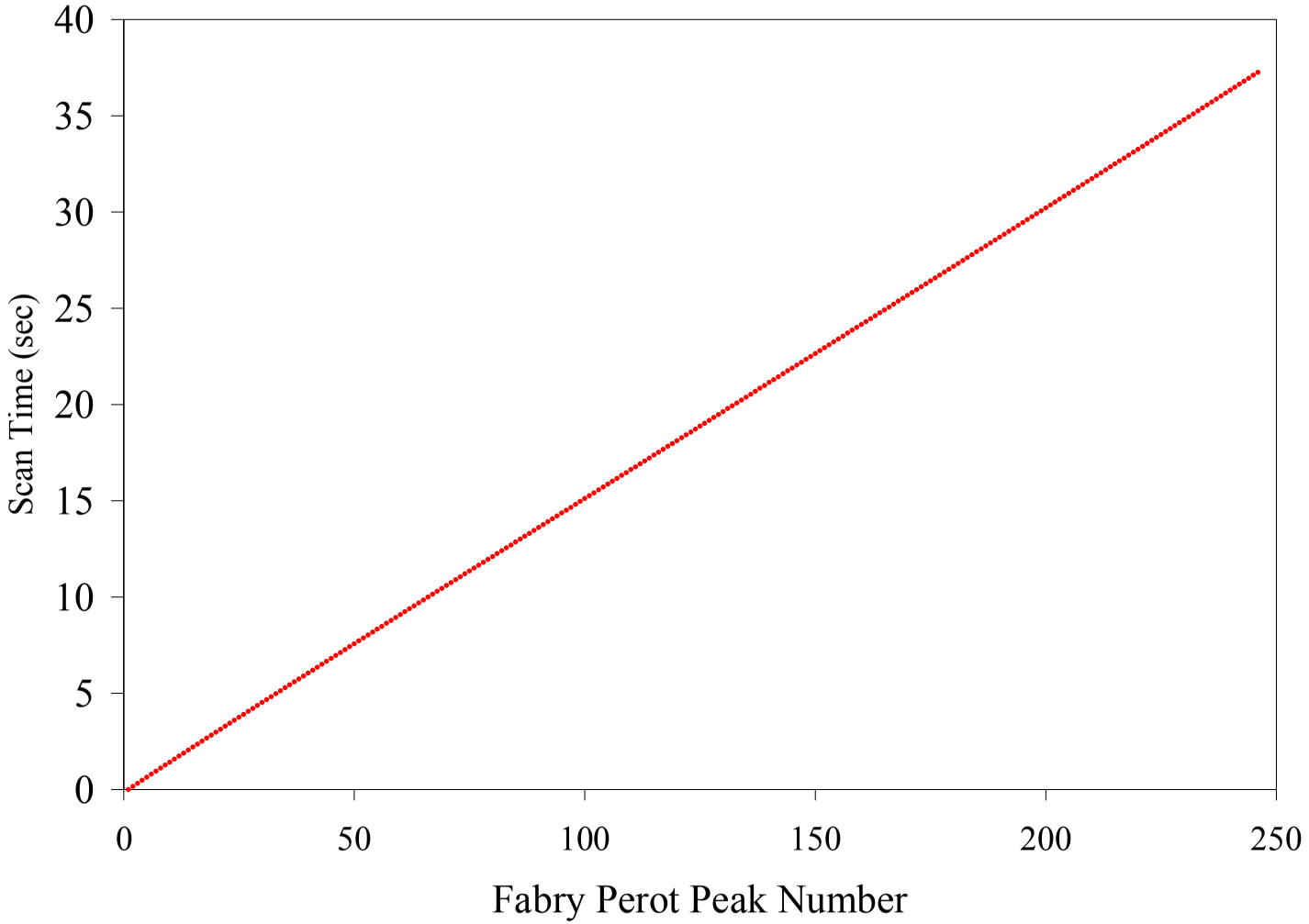

Figure 4.2: Position of Fabry Perot Transmission Peaks during Laser Scan. These data were used to monitor the linearity of the laser frequency scan.

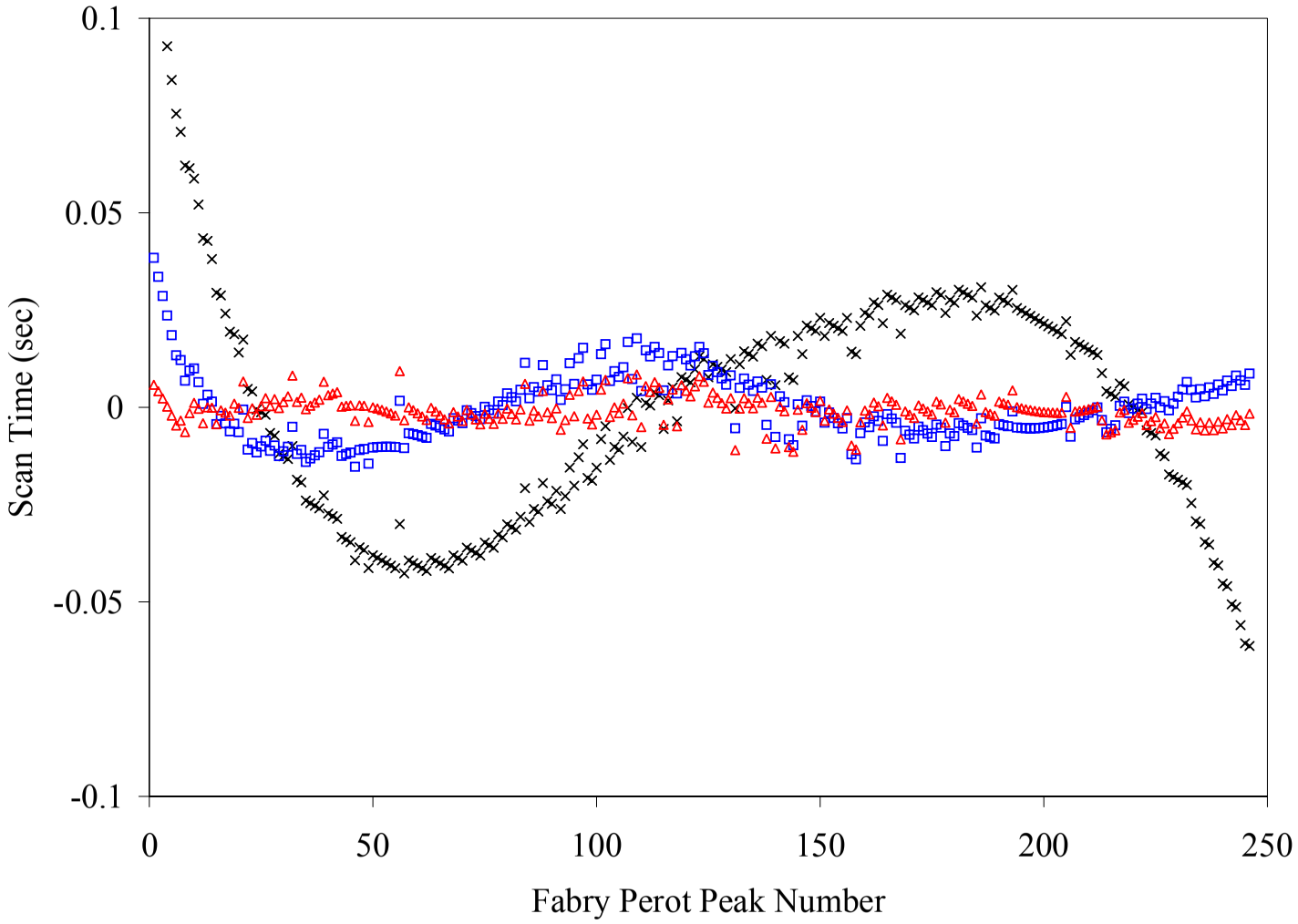

Figure 4.3: Laser Scan Linearity. A polynomial of degree n was fitted to the location of the laser transmission peak centers displayed in Fig. 4.2. The residuals are shown for n=1 (black cross), n=3 (blue square) and n=5 (red triangle).

4.2 Fitting Fluorescence Spectra

Each fluorescence scan consisted of a number of peaks labeled numerically from 1-12 as defined in Fig. 1.1. The peak positions were determined using a Matlab program which fitted the spectra to a sum of N Lorentzian functions given by the following.

$$L(\nu) = \sum_{n=1}^{N} \frac{A_n}{(\nu - \nu_{on})^2 + (\Gamma_n/2)^2} + B \tag{4.1}$$

Here, ν is the frequency, A_n is the amplitude of peak n which is centered at frequency ν_{on} and has a full width at half maximum intensity (FWHM) of Γ_n. B is the background signal caused by laser scatter.

Data obtained by exciting ^{6}Li is shown in Fig. 4.4. The atoms were excited by a laser that passed through an EOM operating at 6.8 GHz. The first peaks labeled 5 and 6 were excited by the frequency shifted laser beam while the second pair of peaks labeled 5 and 6 were excited by the unshifted laser frequency. The PMT voltage was reduced midway through the scan near the 7 GHz mark to avoid saturating the photomultiplier. This can be seen by the slight reduction in the amount of background laser scatter.

The data were fitted as follows. First, the sum of Lorentzian functions given by equation 4.1 were fitted to peaks 1 to 4. This was then separately repeated for the first pair and the later pair of peaks labeled 5 and 6. This method was much faster than fitting the entire spectrum at once which involved a much larger number of

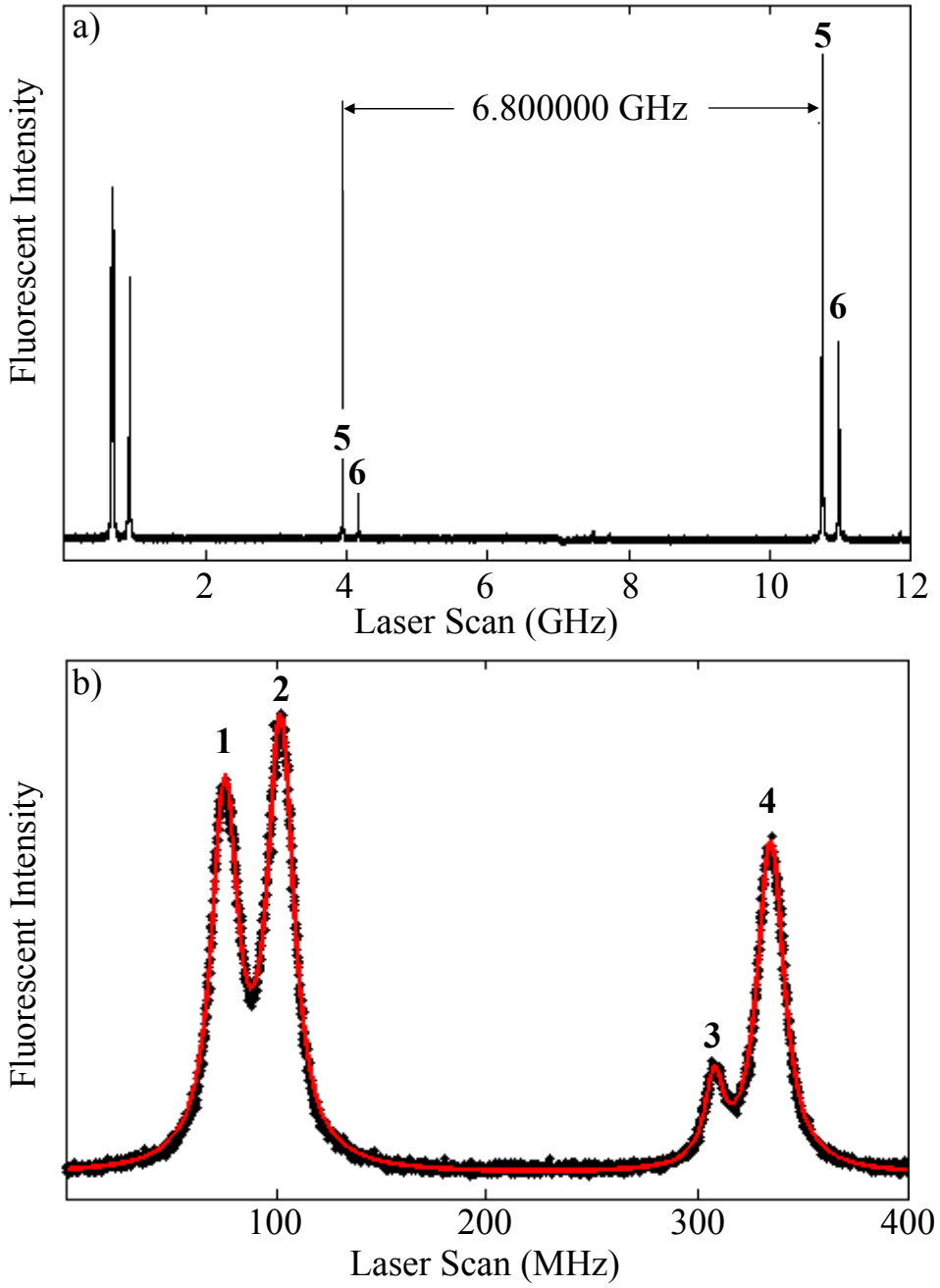

Figure 4.4: Sample ^{6}Li Laser Scan. (**a**) shows a scan where the laser excited transitions 1-6 illustrated in Fig. 1.1 using an electro-optic modulation frequency of 6.800000 GHz. The first four peaks are shown in (**b**) along with the red curve fitted to the data as is discussed in the text.

Table 4.1: Free Spectral Range (FSR) of Fabry Perot Etalon observed on various days. The uncertainty is the standard deviation of the data about the average value.

Run Date	Sample	Number of Runs	FSR (MHz)
Oct. 6	^{6}Li	59	149.736
Oct. 25		62	149.708
Oct. 27		47	149.693
Dec. 2		32	149.699
Dec. 6		92	149.676
Nov. 24	Natural Li	69	149.632
Dec. 9		95	149.721
Dec. 14		28	149.761
Jan. 11		75	149.761
Result			149.710 ± 0.041

points, most of which were baseline background.

Negligible difference in the peak positions was found if all of the peaks widths were specified to be equal. The observed peak widths were found to equal about twice the natural linewidth of 5.8 MHz [25, 26]. The broadening can result from a number of mechanisms including residual Doppler width and power broadening. Data were taken using a laser intensity comparable to the saturation intensity of 5.1 mW/cm^2 [51].

Peaks 5 and 6 that each occur twice in the spectrum shown in Fig. 4.4 permitted the calibration of the Fabry Perot etalon. The interval separating these peaks was first determined in units of FSR. The electro-optic modulation frequency then converts FSR into MHz. This was done for each laser scan. Each data point was found to correspond to a frequency of 12 kHz. Hence, the experiment did not rely on a single calibration of the Fabry Perot etalon at the beginning of the experiment. This technique avoided vibrations, temperature and pressure fluctuations that could perturb the etalon length. Table 4.1 shows the FSR observed on different days. The FSR was found to vary by less than about one part in 4×10^4 during a time period of three months.

Data obtained by exciting natural lithium are shown in Fig. 4.5. Peaks 5 to 10 were fitted separately from peaks 11 and 12 which are shown in Figs. 4.6 and 4.7. Peak 11 results from excitation of the $2S_{1/2}$ F=2 ground state hyperfine level to the $2P_{3/2}$ F= 1, 2, 3 levels. These three transitions overlap as the $2P_{3/2}$ hyperfine splitting is comparable to the 5.8 MHz transition natural linewidth. Peak 11 was therefore fitted using three Lorentzian functions having center frequencies that differed by the hyperfine intervals separating the $2P_{3/2}$ F=1 and 2 as well as F=2 and 3 levels. The amplitudes of the three Lorentzians were however varied by the fitting program.

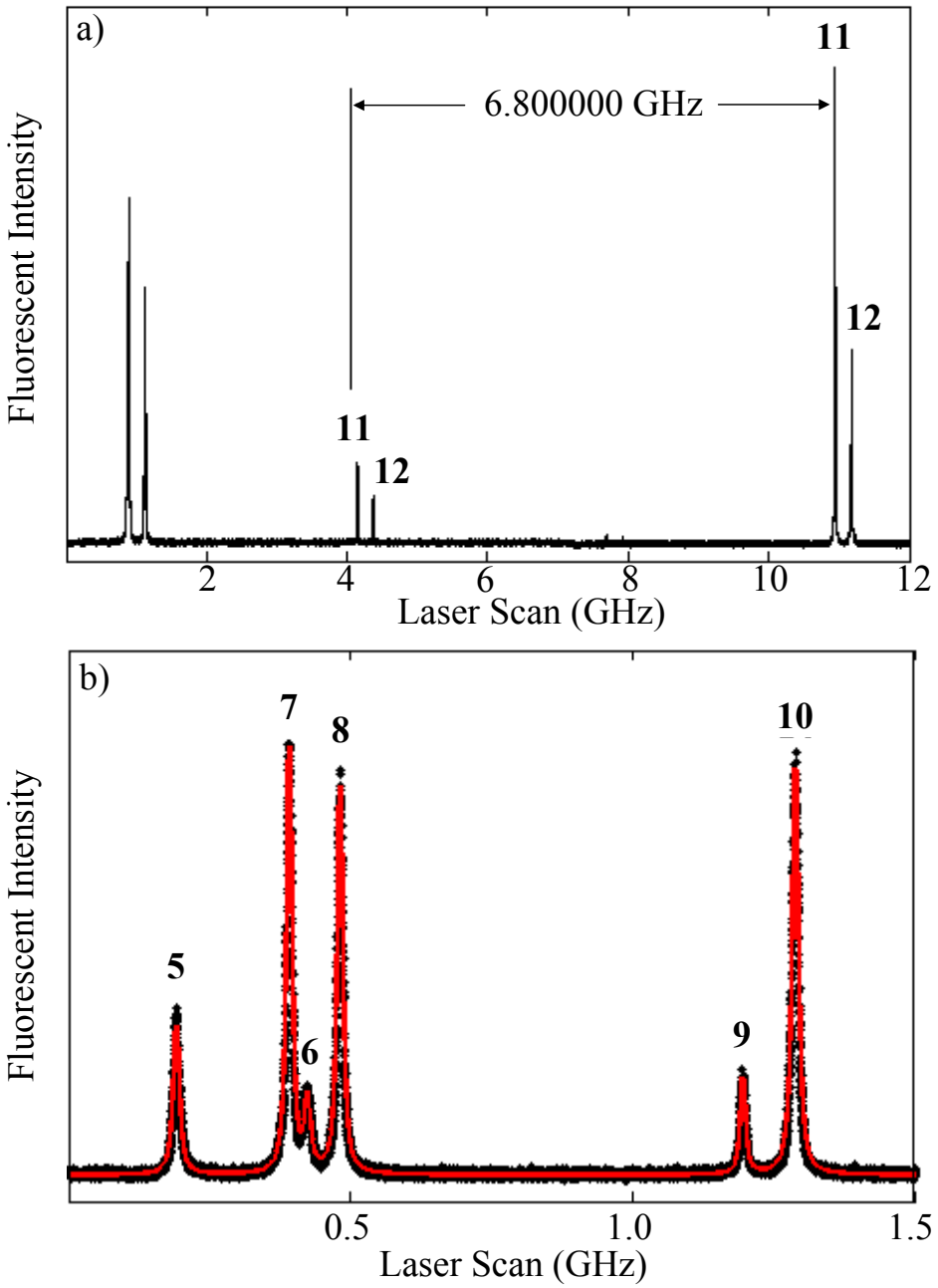

Figure 4.5: Sample Natural Li Laser Scan. (**a**) shows a scan where transitions 5 and 6 of ^{6}Li and transitions 7-12 of ^{7}Li were excited using an electro-optic modulation frequency of 6.800000 GHz. (**b**) shows the first six peaks where the red curve is fitted to the data as is discussed in the text.

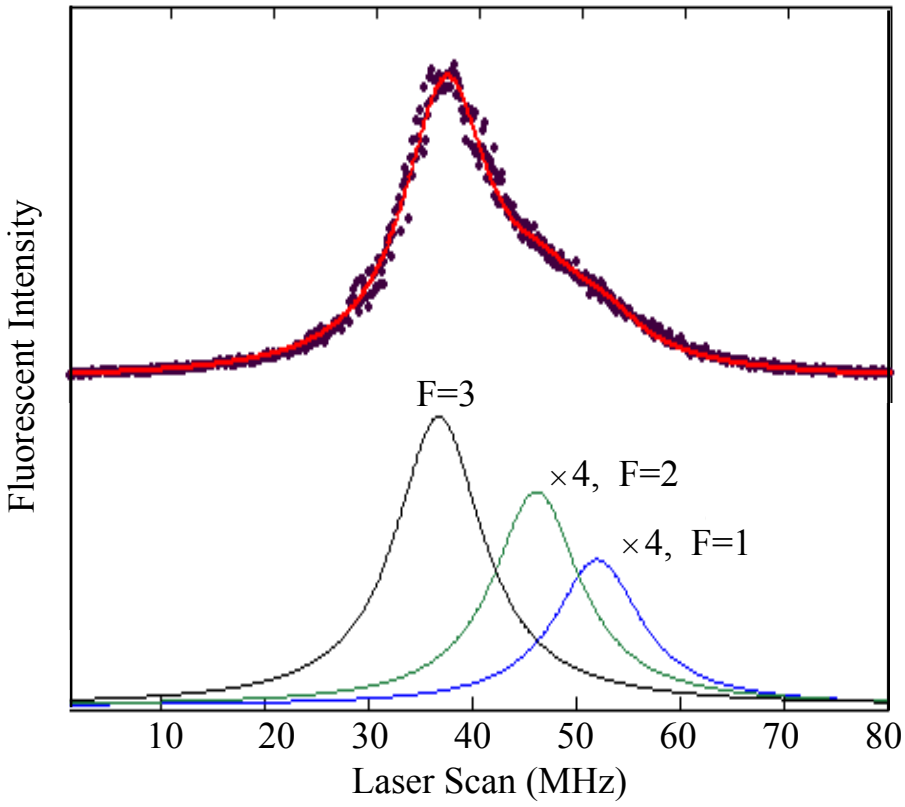

Figure 4.6: Peak 11. The red fitted curve is comprised of 3 peaks produced by the $2P_{3/2}$ state hyperfine levels F = 1, 2, 3 as discussed in the text. The fluorescence contributions from the $2P_{3/2}$ F=1, 2 hyperfine levels hyperfine levels are magnified by a factor of 4.

For Peak 11, about 80% of the fluorescence originates from the radiative decay of the F=3 hyperfine level of the $2P_{3/2}$ state. This peak is generated by excitation of the $2S_{1/2}$ F=2 level by a linearly polarized laser beam. The fraction of atoms excited to the $2P_{3/2}$ F=1, 2 and 3 levels is estimated to be 5%, 25% and 70%, respectively using the relevant transition strengths [56]. Moreover, electric dipole selection rules only allow the $2P_{3/2}$ F=3 level to radiatively decay to the F=2 ground state level

from which it can be re-excited by the laser. In contrast, the $2P_{3/2}$ F=1 and 2 levels can also decay to the F=1 ground state level which is not in resonance with the laser beam. Hence, the repeated excitation followed by radiative decay of the $2P_{3/2}$ state as the atom traverses the laser beam increases the relative contribution of the F=3 level to peak 11.

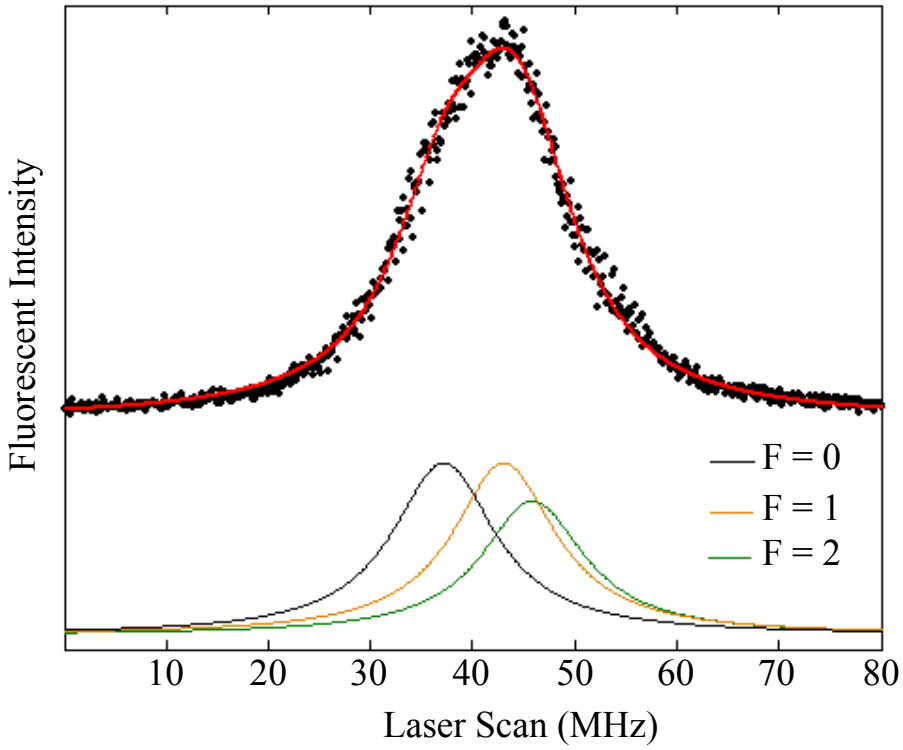

Figure 4.7: Peak 12. The red fitted curve is comprised of 3 peaks produced by the $2P_{3/2}$ state hyperfine levels F = 0, 1, 2 as discussed in the text.

Peak 12 is produced by exciting the $2S_{1/2}$ F=1 ground state hyperfine level to the $2P_{3/2}$ F=0, 1, 2 levels. It was fitted in similar fashion as peak 11 by specifying the relative center frequencies to equal the hyperfine intervals separating the upper state

hyperfine intervals. The resulting fit is shown in Fig. 4.7.

4.3 Determination of Hyperfine Splitting of ^{6,7}Li Ground and $2P_{1/2}$ States

The experiment was tested by measuring the ground and excited state hyperfine intervals and comparing the results to published values. The ^{6}Li $2S_{1/2}$ hyperfine splitting equals the interval separating peaks 1 and 3 and also peaks 2 and 4. It was measured as shown in Table 4.2. The uncertainty represents one standard deviation of the data about the average value. The results agrees very well with the value obtained using the atomic beam magnetic resonance method (ABMR) [45]. Similarly, the ^{7}Li $2S_{1/2}$ hyperfine splitting which equals the frequency interval separating peaks 7 and 9 and also peaks 8 and 10, was found as shown in Table 4.3. This result is also consistent with the corresponding ABMR result.

The hyperfine splittings of the excited ^{6,7}Li $2P_{1/2}$ states were also examined. Table 4.4 shows the ^{6}Li $2P_{1/2}$ magnetic dipole hyperfine constant a which was found by measuring the interval separating peaks 1 and 2 which equals $1.5a(^6\text{Li } 2P_{1/2})$. The result is compared to previous measurements in Table 4.5. Similarly, Table 4.6 gives the result for $a(^7\text{Li } 2P_{1/2})$ found by measuring the separation of peaks 7 and 8 and also 9 and 10 which equals $2a(^7\text{Li } 2P_{1/2})$. Tables 4.5 and 4.7 show the present results agreed closely with the most accurate values obtained in our previous work and by other groups using different techniques.

Table 4.2: Determination of ^{6}Li Ground State Hyperfine Splitting.

Run Date	Peak 3 - Peak 1 (MHz)	Peak 4 - Peak 2 (MHz)	Average (MHz)
Sept. 29		227.531 ± 0.483	227.531 ± 0.483
Oct. 6	228.236 ± 0.317	227.249 ± 0.399	227.854 ± 0.248
Oct. 25	228.166 ± 0.527	227.786 ± 0.575	227.993 ± 0.389
Oct. 27	228.695 ± 0.652	227.807 ± 0.671	228.264 ± 0.468
Dec. 2	228.943 ± 0.171	227.501 ± 0.224	228.412 ± 0.136
Dec. 6	228.786 ± 0.203	227.706 ± 0.198	228.233 ± 0.142
Final Result [18]			228.226 ± 0.086
ABMR [45]			228.205259

Table 4.3: Determination of ^{7}Li Ground State Hyperfine Splitting.

Run Date	Peak 9 - Peak 7 (MHz)	Peak 10 - Peak 8 (MHz)	Average (MHz)
Nov. 24	804.020 ± 0.422	803.213 ± 0.393	803.588 ± 0.288
Dec. 9	803.578 ± 0.141	803.639 ± 0.172	803.603 ± 0.109
Dec. 14	803.561 ± 0.163	803.759 ± 0.147	803.670 ± 0.109
Jan. 11	803.157 ± 0.193	803.301 ± 0.209	803.223 ± 0.142
Final Result [18]			803.544 ± 0.066
ABMR [45]			803.504087

Table 4.4: Determination of Magnetic Dipole Hyperfine Constant ^{6}Li $2P_{1/2}$ State

Run Date	a($2P_{1/2}$) (MHz)
Sept. 29	17.388 ± 0.169
Oct. 6	17.530 ± 0.160
Oct. 25	16.950 ± 0.214
Oct. 27	17.361 ± 0.201
Dec. 2	17.473 ± 0.048
Dec. 6	17.273 ± 0.078
Final Result	17.407 ± 0.037

Table 4.5: Comparison of Determinations of Magnetic Dipole Hyperfine Constant of ^{6}Li $2P_{1/2}$ State

Method	Result (MHz)
ODR [3]	17.48 ± 0.15
ODR [24]	17.375 ± 0.018
LC [7]	17.8 ± 0.3
LAB [8]	16.8 ± 0.7
LAB [40]	17.394 ± 0.004
LABEO [11]	17.386 ± 0.031
This Work	17.407 ± 0.037

Table 4.6: Determination of Magnetic Dipole Hyperfine Constant of ^{7}Li $2P_{1/2}$ State

Run Date	Peaks 7 & 8 (MHz)	Peaks 9 & 10 (MHz)	Average (MHz)
Nov. 24	46.040 ± 0.176	45.741 ± 0.206	45.914 ± 0.134
Dec. 9	45.898 ± 0.073	45.929 ± 0.054	45.918 ± 0.043
Dec. 14	45.845 ± 0.059	45.944 ± 0.061	45.893 ± 0.042
Jan. 11	45.844 ± 0.076	45.918 ± 0.093	45.874 ± 0.059
Final Result			45.899 ± 0.026

Table 4.7: Magnetic Dipole Hyperfine Constant of ^{7}Li $2P_{1/2}$ State. (ODR = Optical Double Resonance, LAB = Laser Atomic Beam, LABEO = Laser Atomic Beam using Electro-Optic modulation, FCPC = Full Core Plus Correlation, MCHF = MultiConfigurational Hartree Fock, MBPT = Many Body Perturbation Theory)

	Method	Result (MHz)
Experiment	ODR [3]	46.17 ± 0.35
	ODR [12]	45.914 ± 0.025
	LAB [8]	46.05 ± 0.30
	LAB [40]	46.024 ± 0.003
	LABEO [11]	46.010 ± 0.025
	This Work	45.899 ± 0.026
Theory	FCPC [57]	45.793
	MCHF [58]	45.984 ± 0.007
	MCHF [59]	45.945
	MBPT [26]	45.916

5 Results

This chapter discusses the determination of the fine structure of the ^{6}Li and ^{7}Li 2P state. The result is compared to measurements obtained by other experiments and that computed from theory. Next, the ^{6,7}Li D1 and D2 isotope shifts are found. This data in conjunction with theoretical results computed using the Hylleraas Variational technique determine the relative ^{6,7}Li nuclear charge radius.

5.1 Fine Structure

The Li 2P fine structure was determined by examining the separation of the D1 and D2 transitions illustrated in Fig. 1.1. The fine structure interval equals the difference between the so called center of gravities of the $2P_{1/2}$ and $2P_{3/2}$ states. This was obtained using the hyperfine splittings of the ground and excited states which are well known [24].

A complication arises for the $2P_{3/2}$ state in both ^{6,7}Li, since the hyperfine splitting is less than or comparable to the 5.8 MHz full width at half maximum (FWHM) natural linewidth. Hence, peaks 5 and 6 in ^{6}Li, and 11 and 12 in ^{7}Li resulted from the simultaneous excitation of more than a single hyperfine level. For example, fluorescence producing peak 5 resulted from the decay of the $2P_{3/2}$ F=1/2, 3/2 and 5/2 levels. The frequency of peak 5 therefore depended on the fractions of fluorescence arising from the various hyperfine levels. These fluorescent fractions were affected by

Table 5.1: Determination of the ^{6}Li 2P Fine Structure. This was found by measuring the interval separating either peaks 5 or 6 from peaks 1 to 4. The hyperfine splittings of the upper and lower state were used to find the intervals relative to the center of gravity of the upper and lower state as is described in the text.

		2P Fine Structure Interval		
Date	Peak i	Peak 5 (MHz)	Peak 6 (MHz)	Average (MHz)
Oct. 6	1	$10,053.063 \pm 0.299$	$10,053.029 \pm 0.249$	$10,053.043 \pm 0.191$
	2	$10,052.879 \pm 0.314$	$10,052.845 \pm 0.273$	$10,052.860 \pm 0.206$
	3	$10,053.010 \pm 0.269$	$10,052.995 \pm 0.274$	$10,053.003 \pm 0.192$
	4	$10,052.827 \pm 0.318$	$10,052.813 \pm 0.329$	$10,052.820 \pm 0.229$
Oct. 25	1	$10,052.129 \pm 0.661$	$10,052.693 \pm 0.670$	$10,052.407 \pm 0.471$
	2	$10,052.840 \pm 0.715$	$10,053.404 \pm 0.724$	$10,053.118 \pm 0.509$
	3	$10,052.567 \pm 0.672$	$10,053.150 \pm 0.681$	$10,052.855 \pm 0.478$
	4	$10,052.200 \pm 0.664$	$10,052.780 \pm 0.674$	$10,052.486 \pm 0.473$
Dec. 2	1	$10,052.740 \pm 0.237$	$10,053.264 \pm 0.170$	$10,053.086 \pm 0.138$
	2	$10,052.600 \pm 0.245$	$10,053.123 \pm 0.172$	$10,052.950 \pm 0.141$
	3	$10,053.002 \pm 0.252$	$10,053.525 \pm 0.188$	$10,053.338 \pm 0.151$
	4	$10,052.304 \pm 0.281$	$10,052.828 \pm 0.238$	$10,052.609 \pm 0.182$
Dec. 6	1	$10,052.423 \pm 0.267$	$10,053.229 \pm 0.259$	$10,052.838 \pm 0.186$
	2	$10,052.625 \pm 0.265$	$10,053.431 \pm 0.267$	$10,053.025 \pm 0.188$
	3	$10,052.842 \pm 0.284$	$10,053.648 \pm 0.264$	$10,053.274 \pm 0.193$
	4	$10,052.124 \pm 0.277$	$10,052.931 \pm 0.267$	$10,052.542 \pm 0.192$
Final Result				$10,052.964 \pm 0.050$

optical pumping. An atom, initially entering the laser beam, can be assumed to have all of its ground state hyperfine sublevels equally populated. The effect of repeated excitation and radiative decay as the atom passes through the linearly polarized laser beam changed the relative populations of the ground state magnetic sublevels having different values of $|m_F|$ where m_F is the magnetic sublevel quantum number.

Optical pumping can depend on a variety of factors such as the laser power, detuning from resonance, atom speed, etc making it difficult to model reliably for a high precision measurement. However, peak 6 was unaffected by the optical pumping since it arose from excitation of the ^{6}Li $2S_{1/2}$ F=1/2 state. The fluorescent fractions contributing to peak 6 originating from the $2P_{3/2}$ F=1/2 and 3/2 hyperfine levels were calculated as discussed in Appendix C to be 47.06% and 52.94%, respectively. This effect shifted peak 6 above the $2P_{3/2}$ center of gravity by +1.970 MHz, as indicated in Fig. 1.1. It should be emphasized that this shift was the only one that was estimated, whereas all other shifts used in the data analysis such as the shift of peak 5 from the $2P_{3/2}$ center of gravity were determined from experimental observation.

The shift of peak 5 below the $2P_{3/2}$ center of gravity was observed for each scan by subtracting the ground state hyperfine splitting and the aforementioned shift of peak 6 from the frequency interval separating peaks 5 and 6. The shifts of peaks 5 and 6 from the $2P_{3/2}$ center of gravity were comparable in magnitude but opposite in sign. The effect of these shifts of peaks 5 and 6 on the determination of the ^{6}Li 2P fine structure was minimized by averaging the values obtained using the two

Table 5.2: Determination of ^{7}Li 2P Fine Structure. This was found by measuring the interval separating either peaks 11 or 12 from peaks 7 to 10. The hyperfine splittings of the upper and lower state were used to find the intervals relative to the center of gravity of the upper and lower state as is described in the text.

Date	Peak i	2P Fine Structure Interval	
		Peak 11	Peak 12
		MHz	MHz
Dec. 9	7	$10,053.298 \pm 0.205$	$10,053.236 \pm 0.229$
	8	$10,053.280 \pm 0.228$	$10,053.439 \pm 0.273$
	9	$10,053.392 \pm 0.230$	$10,053.161 \pm 0.219$
	10	$10,053.188 \pm 0.189$	$10,053.115 \pm 0.223$
Dec. 14	7	$10,053.531 \pm 0.395$	$10,053.529 \pm 0.362$
	8	$10,053.650 \pm 0.388$	$10,053.648 \pm 0.334$
	9	$10,053.383 \pm 0.353$	$10,053.380 \pm 0.325$
	10	$10,053.284 \pm 0.372$	$10,053.282 \pm 0.348$
Jan. 11	7	$10,052.293 \pm 0.315$	$10,052.236 \pm 0.381$
	8	$10,052.482 \pm 0.311$	$10,052.449 \pm 0.379$
	9	$10,052.663 \pm 0.312$	$10,052.560 \pm 0.377$
	10	$10,052.703 \pm 0.292$	$10,052.639 \pm 0.363$
Average		$10,053.116 \pm 0.079$	$10,053.123 \pm 0.086$
Final Result		$10,053.119 \pm 0.058$	

peaks as shown in Table 5.1. The uncertainty of each day's result listed in Tables 5.1 and 5.2 equals one standard deviation of the data about the average value. The laser frequency was less stable on Oct. 25 than on the other days causing a larger uncertainty.

The ^{7}Li 2P fine structure was determined by examining the separation of peaks 11 and 12 from peaks 7 to 10. The center of gravity of the $2P_{3/2}$ state was found by fitting peaks 11 and 12 to linear combinations of Lorentzian functions as described in the previous chapter. The values found for the ^{7}Li 2P fine structure splitting using peaks 11 and 12 were in excellent agreement and are listed in Table 5.2.

Table 5.3 compares fine structure results found for the various experiments with that computed by theory. Considerable disagreement exists among experiments that used the LAB technique to determine the 2P fine structure. This disagreement is believed to be due to difficulties in calibrating the Fabry Perot interferometer used to measure the change in laser frequency as was discussed in Chapter 2. It is interesting to determine the 2P fine structure discarding the results of these LAB experiments. For ^{6}Li, averaging the results of the Level Crossing experiment and this work gives a value of $10,052.954 \pm 0.049$ MHz. For ^{7}Li, the result of the present work is consistent with those of the Level Crossing and Optical Double Resonance experiments. The average of these three results is $10,053.154 \pm 0.040$ MHz. These results are about 2 MHz above theory which did not take into account mass independent higher order terms. The theoretical results listed in Table 5.3 have a computational uncertainty

Table 5.3: Comparison of Experimental and Theoretical Fine Structure Results. The first uncertainty listed for the theoretical result is the calculational uncertainty while the second number is the estimated effect of higher order terms not taken into account.

Interval	Experiment (MHz)	Method	Theory[60] (MHz)
^{6}Li 2P	$10,052.76 \pm 0.22$	LC [7]	$10,050.85 \pm 0.02 \pm 3$
	$10,050.2 \pm 1.5$	LAB [8]	
	$10,051.62 \pm 0.20$	LAB [9]	
	$10,052.862 \pm 0.067$	LAB [10]	
	$10,053.044 \pm 0.091$	LABEO [11]	
	$10,052.964 \pm 0.050$	This Work [18]	
^{7}Li 2P	$10,053.24 \pm 0.22$	LC [7]	$10,051.24 \pm 0.02 \pm 3$
	$10,053.184 \pm 0.058$	ODR [12]	
	$10,056.6 \pm 1.5$	LAB [8]	
	$10,053.2 \pm 1.5$	LAB [13]	
	$10,053.40 \pm 0.20$	LAB [9]	
	$10,051.999 \pm 0.041$	LAB [10]	
	$10,052.37 \pm 0.11$	LABEO [11]	
	$10,053.119 \pm 0.058$	This Work [18]	

as well as a 3 MHz uncertainty due to these higher order effects. Similar terms in two electron systems have been found to have a magnitude of several MHz [20].

5.2 D1 and D2 Isotope Shifts

The simplest way to determine the D1 isotope shift is to measure the interval separating peaks 1 to 4 from peaks 7 to 10 in a scan of natural lithium. However, the ^{6}Li peaks are more than an order of magnitude smaller than the ^{7}Li peaks when natural lithium is loaded into the oven. One can add ^{6}Li to the natural lithium sample but this increases the overlap of peaks 6, 7, and 8 as shown in Fig. 4.5. The D1 isotope shift was therefore determined by measuring the intervals separating peaks 7 to 10 from peak 5 obtained using a natural lithium sample. Next, the intervals separating peaks 1 to 4 from peak 5 obtained using ^{6}Li were found. The D1 isotope shift was then found by adding the two intervals and using the ground and excited state hyperfine splittings to determine the frequency intervals of peak 5 to the ^{6,7}Li $2P_{1/2}$ center of gravities as shown in Table 5.4.

Table 5.5 compares the isotope shift results obtained by various experiments. The Li^+ $2\ ^3S_1 \rightarrow 2\ ^3P_{0,1,2}$ transitions were studied by the Riis group [5]. The D1 and D2 lines have been examined by the Sansonetti group using FM spectroscopy [14]. The laser atomic beam technique has been used by Windholz in two different experiments [8, 13] as well as by Das et al [10]. The three results for the Li $2^2S_{1/2} \rightarrow 3^2S_{1/2}$

Table 5.4: Determination of ^{6,7}Li D1 Isotope Shift. This was found by measuring the interval separating either peaks 7 to 10 from peak 5 as well as the interval separating peak 5 to peaks 1 to 4. The hyperfine splittings of the upper and lower state were used to find the intervals relative to the center of gravity (CG) of the upper and lower state as is described in the text.

Date	Peak	^{7}Li $2P_{1/2}$ CG - Peak 5 (MHz)	Date	Peak	Peak 5 - ^{6}Li $2P_{1/2}$ CG (MHz)
Nov. 24	7	558.036 ± 0.450	Oct. 6	1	9975.800 ± 0.314
	8	558.231 ± 0.309		2	9975.567 ± 0.311
	9	558.645 ± 0.392		3	9975.767 ± 0.293
	10	558.108 ± 0.396		4	9975.536 ± 0.351
Dec. 9	7	558.139 ± 0.150	Oct. 25	1	9975.769 ± 0.502
	8	557.988 ± 0.163		2	9976.341 ± 0.491
	9	558.212 ± 0.132		3	9976.174 ± 0.598
	10	558.050 ± 0.148		4	9975.791 ± 0.569
Dec. 14	7	558.734 ± 0.145	Dec. 2	1	9975.523 ± 0.125
	8	558.403 ± 0.116		2	9975.330 ± 0.136
	9	558.791 ± 0.175		3	9975.798 ± 0.174
	10	558.658 ± 0.156		4	9975.035 ± 0.194
Jan. 11	7	558.950 ± 0.153	Dec. 6	1	9975.851 ± 0.218
	8	558.531 ± 0.187		2	9975.997 ± 0.219
	9	558.492 ± 0.224		3	9976.208 ± 0.219
	10	558.306 ± 0.207		4	9975.458 ± 0.216
Average		558.417 ± 0.044			9975.613 ± 0.056
Final Result			$10,534.039 \pm 0.070$		

transition were all obtained by the GSI/TRIUMF group [15–17]. The table also lists the result of a previous experiment using the LABEO result made by our group [11].

It is disconcerting that the LAB experiments yield conflicting results. The D1 isotope shift obtained by this experiment agrees with that found by Walls et al [11] but has half the uncertainty. The D2 isotope shift listed in Table 5.5 for the present work was computed from the D1 isotope shift using the ^{6,7}Li 2P fine structure splittings as is illustrated in Fig. 1.1. The D2 isotope shift uncertainty is therefore larger since the various uncertainties were added in quadrature.

5.3 Relative Nuclear Charge Radius

One way to check experimental error claims is to find the field shift and the relative nuclear charge radius squared which is defined as follows [61].

$$\Delta R_c^2 = R_c^2(^6\mathrm{Li}) - R_c^2(^7\mathrm{Li}) \tag{5.1}$$

As was discussed in Chapter 1, ΔR_c^2 can be determined using

$$\Delta R_c^2 = (\delta\nu_{jk} - \delta E_{jk})/C_{jk} \tag{5.2}$$

where $\delta\nu_{jk}$ is the measured isotope shift for the transition between states j and k, δE_{jk} is the calculated isotope shift difference for the two states excluding the nuclear size correction and C_{jk} is proportional to the square of the electron wavefunction at

Table 5.5: Measured Isotope Shifts, Field Shift and Determination of Relative Nuclear Charge Radius Squared

Method	Transition	Isotope Shift (MHz)	Field Shift (MHz)	ΔR_c^2 (fm^2)
LIB [5]	Li^+ $2\ ^3S_1 \rightarrow 2\ ^3P_0$	$34,747.73 \pm 0.55$	7.56 ± 0.55	0.78 ± 0.06
	Li^+ $2\ ^3S_1 \rightarrow 2\ ^3P_1$	$34,747.46 \pm 0.67$	7.59 ± 0.67	0.78 ± 0.07
	Li^+ $2\ ^3S_1 \rightarrow 2\ ^3P_2$	$34,748.91 \pm 0.62$	6.20 ± 0.62	0.64 ± 0.06
FM [14]	D1 Line	$10,532.9 \pm 0.6$	0.8 ± 0.6	0.32 ± 0.24
	D2 Line	$10,533.3 \pm 0.5$	0.8 ± 0.5	0.32 ± 0.20
LAB [8]	D1 Line	$10,534.3 \pm 0.3$	2.19 ± 0.3	0.89 ± 0.12
	D2 Line	$10,539.9 \pm 1.2$	7.39 ± 1.2	3.01 ± 0.49
LAB [9]	D1 Line	$10,533.13 \pm 0.15$	1.02 ± 0.15	0.41 ± 0.06
	D2 Line	$10,534.93 \pm 0.15$	2.42 ± 0.15	0.99 ± 0.06
LAB[10]	D1 Line	$10,534.215 \pm 0.039$	2.10 ± 0.04	0.86 ± 0.02
	D2 Line	$10,533.352 \pm 0.068$	0.85 ± 0.07	0.34 ± 0.03
LABEO [11]	D1 Line	$10,534.26 \pm 0.13$	2.15 ± 0.13	0.87 ± 0.05
This Work [18]	D1 Line	$10,534.039 \pm 0.070$	1.93 ± 0.07	0.78 ± 0.03
	D2 Line	$10,534.194 \pm 0.104$	1.69 ± 0.10	0.69 ± 0.04
LAB [15]	D1 Line	$10,533.160 \pm 0.068$	1.05 ± 0.07	0.43 ± 0.03
	Li $2\ ^2S_{1/2} \rightarrow 3\ ^2S_{1/2}$	$11,453.734 \pm 0.030$	0.91 ± 0.03	0.58 ± 0.02
LAB [16]	Li $2\ ^2S_{1/2} \rightarrow 3\ ^2S_{1/2}$	$11,453.95 \pm 0.13$	1.13 ± 0.13	0.72 ± 0.08
LAB [17]	Li $2\ ^2S_{1/2} \rightarrow 3\ ^2S_{1/2}$	$11,453.984 \pm 0.020$	1.16 ± 0.02	0.74 ± 0.01

the nucleus.

Table 5.5 lists the values of ΔR_c^2 for the experimentally determined isotope shifts. The results found by Riis et al for the Li^+ $2\ ^3S_1 \rightarrow 2\ ^3P_{0,1,2}$ transitions are mutually consistent. The weighted average of these results is given in Table 5.6. For the Li D lines, the two values of ΔR_c^2 obtained using the frequency modulation technique agree, but are substantially lower and have a larger uncertainty than those obtained by all other experiments. A number of laser atomic beam experiments have yielded D1 and D2 isotope shifts that yield sharply conflicting values for ΔR_c^2. This indicates these experiments have been too optimistic in estimating their error. The results of the present experiment agree with each other and were averaged to give the result shown in Table 5.6.

For the Li $2\ ^2S_{1/2} \rightarrow 3\ ^2S_{1/2}$ transition, the same group has performed three separate experiments [15–17]. Their most recent result disagrees with their initial experiment by about 5 times the combined uncertainties. This discrepancy is attributed to unaccounted systematic error in the interferometric measurements of the original work. Their last two results are consistent and were averaged to give the value listed in Table 5.6.

Table 5.6 shows the values for ΔR_c^2 found for the three transitions are in excellent agreement. The average result for ΔR_c^2 agrees with nuclear theory [62] as well as with the result of an electron scattering experiment but is 25 times more precise than the latter [22]. Taking the square root of the average value of ΔR_c^2 gives a value of

0.861 ± 0.006 fm. Table 5.6 also lists the ^{6}Li nuclear charge radius found using the corresponding value for ^{7}Li which was obtained in an electron scattering experiment [22].

Table 5.6: Determination of the ^{6}Li Nuclear Charge Radius using $R_c(^7\text{Li}) = 2.39 \pm 0.03$ fm.

Transition	ΔR_c^2 (fm^2)	$R_c(^6\text{Li})$ (fm)	Reference
Li^+ $2\ ^3\text{S} \rightarrow 2\ ^3\text{P}$	0.735 ± 0.036	2.539 ± 0.035	[5]
Li D Lines	0.755 ± 0.023	2.543 ± 0.033	this work [61]
Li 2S $\rightarrow$ 3S	0.739 ± 0.013	2.540 ± 0.031	[17]
Average	0.742 ± 0.011	2.540 ± 0.031	
Electron Scattering	0.79 ± 0.25	2.55 ± 0.04	[22]
Nuclear Theory	0.74 ± 0.15	2.54 ± 0.01	[62]

6 Conclusions

This experiment obtained precise values of the lithium 2P fine structure and the isotope shifts of the D1 and D2 lines. The technique is relatively straight forward as it requires an electro-optically modulated laser beam to excite a well collimated neutral atomic beam. This modulation frequency is conveniently specified to high accuracy with a synthesizer. One does not rely on the calibration of a Fabry Perot Etalon to determine the change in laser frequency. The experiment can also be checked by comparing the measured ground state hyperfine splitting to the atomic clock result. A significant advantage of this technique is that one experiment determines the fine and hyperfine splittings of the ground and excited states as well as the isotope shifts. Other methods such as level crossing or optical double resonance only determine one of these quantities.

An experiment is in progress to attempt to improve absolute transition frequency measurements of the Li D lines using the so called femtosecond frequency comb technique [63]. However, the determination of the Li 2P fine structure is limited by the accuracy of the hyperfine splittings of the ^{6,7}Li $2P_{3/2}$ states. It is difficult to improve the magnetic dipole and electric quadrupole constants of this state as the D2 transition linewidth is comparable to the hyperfine splittings.

The results for the ^{6,7}Li 2P fine structure intervals agree with the best results obtained by level crossing and optical double resonance experiments. The observed

values are about 2 MHz above theory. Improving the calculation of the Li 2P fine structure therefore will be an important test of the Hylleraas Variational method applied to a three electron system. The measured isotope shifts enabled the determination of the ^{6,7}Li relative nuclear charge radius. Consistent results were obtained using the D1 and D2 isotope shifts. The values found for ΔR_c^2 were also in excellent agreement with those obtained by experiments that studied the Li^+ 1s2s $^3S_1 \rightarrow$ 1s2p $^3P_{0,1,2}$ and the Li 2 $^2S_{1/2} \rightarrow$ 3 $^2S_{1/2}$ transitions.

In conclusion, the combination of optically measured isotope shifts and the precise calculations of Hylleraas Variational theory determines the relative charge radii of the ^{6,7}Li nuclei with an accuracy of millifermi. It is remarkable that these experiments yield more accurate data than was obtained using electron scattering. Ironically, one now has a better understanding of how an electron in the lithium atom interacts with the nucleus than of how a macroscopic electron beam scatters from a lithium nucleus. This underscores the incredible advances made in both atomic theory and experiment.

A Determination of Positions of Fabry Perot Maxima

The position of the laser transmission peaks through the etalon were found using a computer program written in Mathematica 5.2. A flowchart of the program is shown in Fig. A.1. The datafile consisted of over one million intensity values measured as the laser frequency was scanned. One approach to finding the peak centers would be to fit each peak to an appropriate function such as a Lorentzian or Gaussian curve. This approach was found to be quite time consuming compared to the method described below.

The program has several inputs that are found by first displaying the entire data file. First, the number of laser transmission peaks N is counted. Next, the position of the first peak x_1 was estimated as well as the number points separating the first two peaks Δx. Finally, the threshold intensity I_{thres} was selected to equal half the maximum peak intensity. For each peak i, 3,000 points on either side of the peak position were extracted from the file. A larger number of points was not considered since these intensity values were near the zero baseline. The position of the first point on the left (right) side of the peak x_L (x_R) whose intensity exceeded I_{thres} was found. The position of peak i, x_i, was found by averaging x_L and x_R. The spacing between neighboring peaks Δx was then computed and used to estimate the position of the next peak. The program then looped back to find the exact peak center as described

previously. Finally, the locations of all N peaks were saved.

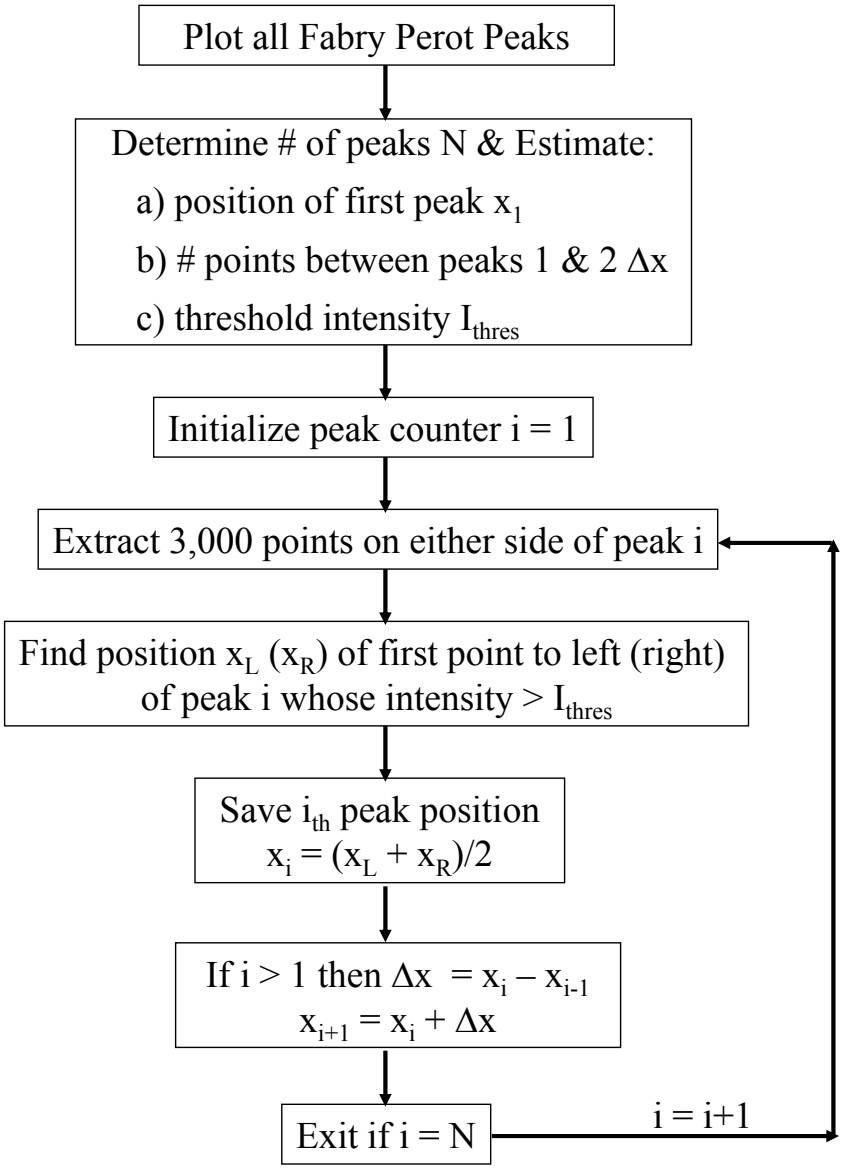

Figure A.1: Flow Chart for Computer Program for Finding Positions of Fabry Perot Maxima

B Computer Program to Linearize Laser Scan

The nonlinearity of the laser frequency scan was taken into account by fitting a 5th order polynomial to the data as follows.

$$y = \sum_{n=0}^{5} a_n x^n \tag{B.1}$$

Here, x is the time of the scan and y is the frequency measured in units of the free spectral range (FSR). The program converted the times at which the fluorescent and Fabry Perot peaks occurred into frequency units. For each fluorescent peak, the 6 unknown coefficients a_n were found by fitting the positions of the 3 nearest Fabry Perot peaks on either side of the fluorescent peak. Fig. B.1 gives a flowchart of the Fortran program. The polynomial B.1 was fitted using subroutine POLYFIT [64].

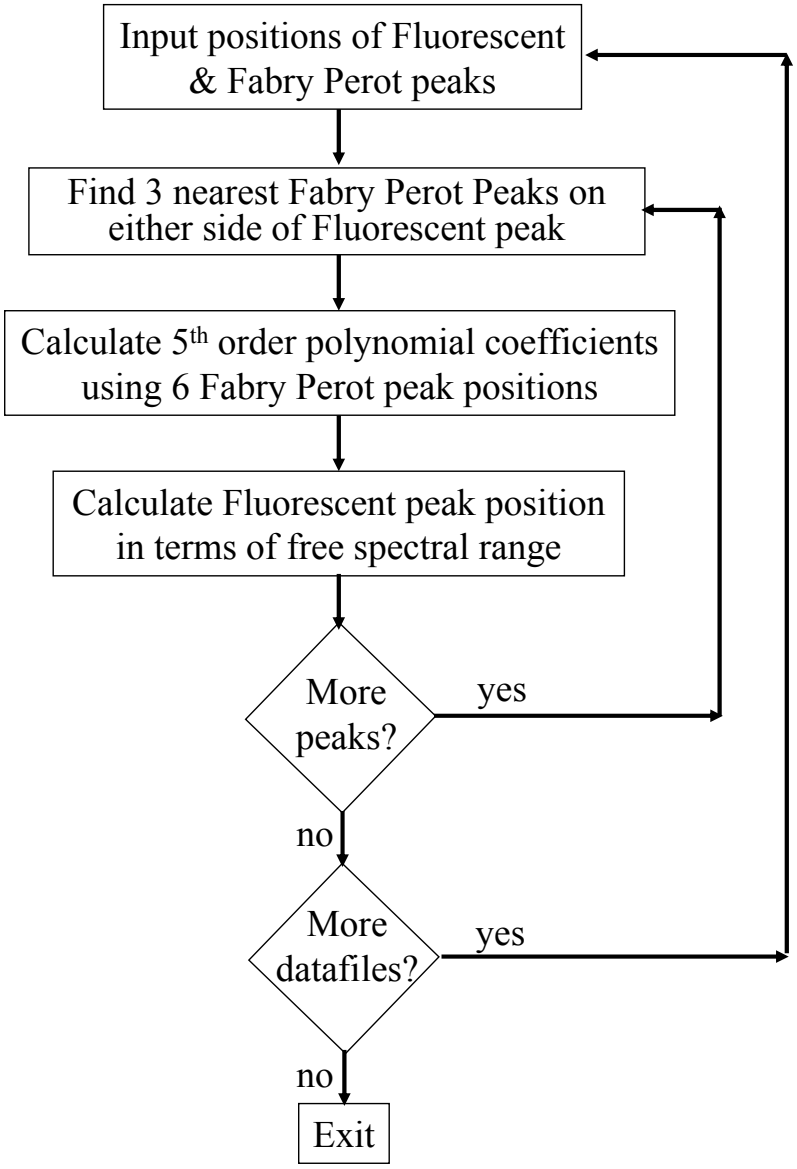

Figure B.1: Flow Chart of Frequency Nonlinearity Compensation Program

```
C       ANALYSIS IS A FREQUENCY NONLINEARITY COMPENSATION CODE
        CHARACTER*25 FILENAME1,FILENAME2,FILENAME3
        REAL*8 FL,FP,RES,X,XFL,DFL,DFP
        DIMENSION FL(100,13),FLOUT(100,13),FP(100,250)
        DIMENSION NUMFP(100),IRUN(100)
        DIMENSION X(6)
        INTEGER ONES,TENS
C       FIRST INITIALIZE FLUORESCENCE PEAK ARRAY.
C       NPKS = NUMBER OF FLUORESCENCE PEAKS
        NPKS=13
        DO 5 I1=1,100
                DO 6 I2=1,NPKS
                        FL(I1,I2)=-9999.99
                        FLOUT(I1,I2)=-9999.99
    6           CONTINUE
    5   CONTINUE

C       FIRST LOAD IN FLUORESCENCE PEAKS FROM ONE DAYS RUNNING
        FILENAME1='LiDec9b.txt'
        OPEN (UNIT=7,FILE=FILENAME1)
        DO 10 I1 = 1, 100
                READ (7,*) IRUN(I1), (FL(I1,I2),I2=1,NPKS)
                I=IRUN(I1)
                IF (I.EQ.0) GO TO 20
   10   CONTINUE
   20   NRUN=I1-1
        WRITE (6,*) NRUN
        CLOSE (7)

C       READ IN FABRY PEROT PEAKS FROM ONE DAYS RUNNING
        FILENAME2='FPDec9\dec9 xx.txt'
        DO 30 I2=1,49
                I22=2*I2
                TENS=I22/10
                ONES=MOD(I22,10)
                FILENAME2(14:14)=CHAR(48+ONES)
                FILENAME2(13:13)=CHAR(48+TENS)
                WRITE (6,*) FILENAME2
                OPEN (UNIT=8, FILE=FILENAME2)
                DO 40 I3=1,250
                        READ (8,*) I, FP(I2,I3)
                        IF (I.EQ.0) GO TO 50
   40           CONTINUE
   50           NUMFP(I2)=I3-1
                CLOSE (8)
   30   CONTINUE
```

```
C       WE NOW FIND NONLINEAR CORRECTION.
   61   DO 60 I1=1,NRUN
                NSTART=3
                DO 70 I2=1,NPKS
                        DFL=FL(I1,I2)
                        IF (DFL.LE.0) GO TO 70
C       FIND THREE FABRY PEROT PEAKS ON EITHER SIDE OF FLUOR. PEAK
                        DO 80 I3=3,NUMFP(I1)-2
                                DFP=FP(I1,I3)
                                IF ((DFL.GT.DFP).AND.(DFL.LT.FP(I1,I3+1))) GO TO 90
    80                  CONTINUE
C       CALL SUBROUTINE TO DO FIND NONLINEAR POLYNOMIAL FIT TO FREQ. SCAN
    90                  X(1)=FP(I1,I3-2)
                        X(2)=FP(I1,I3-1)
                        X(3)=DFP
                        X(4)=FP(I1,I3+1)
                        X(5)=FP(I1,I3+2)
                        X(6)=FP(I1,I3+3)
C       CHECK IF FABRY PEROT PEAKS ARE WELL DEFINED
                        DO 100 I4=1,6
                                IF (X(I4).LT.0) GO TO 70
                                X(I4)=(X(I4)-DFP)/1000.
   100                  CONTINUE
C       POLYFIT DETERMINES FREQUENCY IN UNITS OF FABRY PEROT FSR
                        XFL=(DFL-DFP)/1000.
                        CALL POLYFIT (X,XFL,RES)
                        FLOUT(I1,I2)=RES + I3
    70          CONTINUE
    60  CONTINUE
C       WRITE RESULTS FOR PEAK CENTER FREQUENCIES IN UNITS OF FSR
        FILENAME3='out.txt'
        OPEN (UNIT=9, FILE=FILENAME3)
        DO 400 I1=1,100
                WRITE (9,410) IRUN(I1),(FLOUT(I1,I2),I2=1,NPKS)
   410          FORMAT (I3,1X,13(F12.6,1X))
   400  CONTINUE
        CLOSE (9)
    99  STOP
        END
```

```
      SUBROUTINE POLYFIT (X,XFL,RES)
      DIMENSION A(6), X(6), Y(6)
      DIMENSION SUMX(11), SUMY(6), ARRAY(6,6)
      REAL*8 ARRAY, RES, DELTA, A,SUMX,XUMY,X,Y,XD,XFL,XTERM,XI,YTERM,YI
      Y(1)=-2.
      Y(2)=-1.
      Y(3)=0.
      Y(4)=1.
      Y(5)=2.
      Y(6)=3.
      NTERMS=6
      NPTS=6
      NMAX=2*NTERMS-1

C     INITIALIZE VARIABLES
      DO 200 J1=1,NMAX
            SUMX(J1)=0.
  200 CONTINUE
      DO 210 J2=1,NTERMS
            SUMY(J2)=0.
  210 CONTINUE
C     NOW CALCULATE
      DO 220 J3=1, NPTS
            XI=X(J3)
            YI=Y(J3)
            XTERM=1.
            DO 230 J4=1,NMAX
                  SUMX(J4) = SUMX(J4) + XTERM
                  XTERM=XTERM*XI
  230       CONTINUE
            YTERM=YI
            DO 235 N=1,NTERMS
                  SUMY(N)=SUMY(N)+YTERM
                  YTERM=YTERM*XI
  235       CONTINUE
  220 CONTINUE
      DO 240 J5=1,NTERMS
            DO 250 J6=1, NTERMS
                  N=J5+J6-1
                  ARRAY(J5,J6)=SUMX(N)
  250       CONTINUE
  240 CONTINUE
```

```
      CALL DETERM (ARRAY,DELTA)
      IF (DELTA) 270,260,270
  260 WRITE (6,*) 'Determinant is 0, bugging out'
      DO 280 J7=1, NTERMS
            A(J7)=0.
  280 CONTINUE
      GO TO 290
  270 DO 300 J8=1, NTERMS
            DO 310 J9=1, NTERMS
                  DO 320 J10=1,NTERMS
                        N=J9+J10-1
                        ARRAY(J9,J10)=SUMX(N)
  320               CONTINUE
                    ARRAY(J9,J8)=SUMY(J9)
  310       CONTINUE
            CALL DETERM (ARRAY,A(J8))
            A(J8)=A(J8)/DELTA
  300 CONTINUE
C     LINEARIZED FREQUENCY VALUE IS NOW COMPUTED
  290 RES=0.
      XD=1.
      DO 330 J10=1,NTERMS
            RES=RES+A(J10)*XD
            XD=XD*XFL
  330 CONTINUE
      RETURN
      END
```

```
      SUBROUTINE DETERM (ARRAY,RES)
C     DETERMINANT FINDS THE DETERMINANT OF MATRIX ARRAY WHICH HAS
C     DIMENSION NORDER BY NORDER.  THE FINAL RESULT IS STORED IN RES.
      REAL*8 ARRAY, SA, RES
      DIMENSION ARRAY (6,6)
      NORDER=6
      RES=1.
      DO 510 K=1,NORDER
            IF (ARRAY(K,K)) 530,520,530
  520       DO 540 J=K,NORDER
                  IF (ARRAY(K,J)) 550,540,550
  540       CONTINUE
            RES=0.
            GO TO 560
  550       DO 570 I=K,NORDER
                  SA=ARRAY(I,J)
                  ARRAY(I,J)=ARRAY(I,K)
                  ARRAY(I,K)=SA
  570       CONTINUE
            RES=-RES
  530       RES=RES*ARRAY(K,K)
            IF (K-NORDER) 580,510,510
  580       K1=K+1
            DO 590 I=K1,NORDER
                  DO 600 J=K1, NORDER
                        ARRAY(I,J)=ARRAY(I,J)-ARRAY(I,K)*ARRAY(K,J)/ARRAY(
  600             CONTINUE
  590       CONTINUE
  510 CONTINUE
  560 RETURN
      END
```

C Fluorescence Contributions to Peak 6 of $2P_{3/2}$ F=1/2, 3/2 Hyperfine Levels

The excitation of the ^{6}Li $2S_{1/2}$ F = 1/2 hyperfine level to the $2P_{3/2}$ excited state is shown schematically in Fig. C.1. The laser simultaneously excited the F=1/2, 3/2 hyperfine levels of the excited state since the hyperfine splitting is less than the transition linewidth. The laser was linearly polarized and hence, only transitions for which the azimuthal sublevel quantum number remains unchanged were allowed. The transition strength depends on the square of the the matrix element $\langle \Psi_G | \mu_{EG} | \Psi_E \rangle$ where Ψ_G and Ψ_E are the ground state and excited state wave functions respectively [56]. μ_{EG} is the dipole matrix element described by

$$\begin{aligned} \mu_{EG} &= e(-1)^{1+L'+S+J+J'+I-m_F} \\ &\times \sqrt{(2J+1)(2J'+1)(2F+1)(2F'+1)} \\ &\times \begin{Bmatrix} L' & J' & S \\ J & L & 1 \end{Bmatrix} \begin{Bmatrix} J' & F' & I \\ F & J & 1 \end{Bmatrix} \begin{pmatrix} F & 1 & F' \\ m_F & \Delta m_F & -m'_F \end{pmatrix} \\ &\times \langle \Gamma' L' \parallel r \parallel \Gamma L \rangle \end{aligned} \tag{C.1}$$

Here, e is the electron charge, L, S and J are the orbital, spin and total angular momenta of the electron in the upper (primed) and lower (unprimed) states. I is the nuclear spin while F and F' are the hyperfine quantum numbers of the upper and lower states respectively having azimuthal components m_F and $m_{F'}$. Δm_F is defined to equal $m_F - m_{F'}$. Hence, $\Delta m_F = 0$ for the case of light linearly polarized

along the quantization axis while $\Delta m_F = \pm 1$ for circularly polarized light. The various angular momenta are coupled via $3j$ (round brackets) and $6j$ symbols (curly brackets). $\langle \Gamma' L' \parallel r \parallel \Gamma L \rangle$ is the reduced matrix element which depends on other quantum numbers Γ and Γ' describing the upper and lower states.

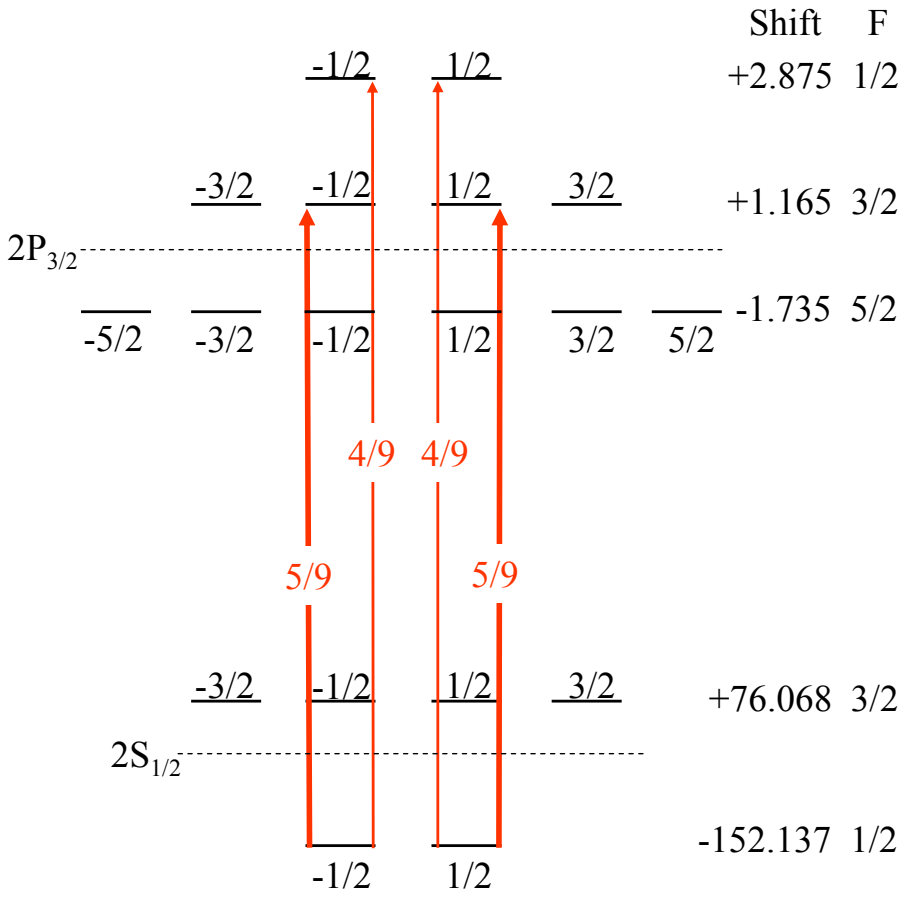

Figure C.1: Excitation of ^{6}Li $2S_{1/2}$ F=1/2 $\rightarrow$ $2P_{3/2}$ Transition by Linearly Polarized Laser Light. The positions of the various hyperfine levels are indicated relative to the state's center of gravity in units of MHz. The relative transition strengths are given in red and denote the coupling of the laser to the transition as described in the text.

Peak 6 was produced by the radiative decay of the $2P_{3/2}$ F=1/2, 3/2 levels. The photomultiplier was oriented along the laser polarization axis and therefore only detects photons produced by a transition obeying the selection rule $\Delta m_F = \pm 1$. Fig. C.2 shows the radiative decays of the $2P_{3/2}$ F=1/2 $m = -1/2$ level producing circularly and linearly polarized light. The relative strength of these various decays is proportional to the matrix element given in equation (C.1). Hence, for the $2P_{3/2}$ F = 1/2 level, the photomultiplier detects a maximum $(15 + 5 + 160)/(15 + 5 + 160 + 10 + 80) = 2/3$ of all photons produced. Fig. C.3 shows the radiative decays of the $2P_{3/2}$ F=3/2 $m = -1/2$ level. The maximum fraction of photons detected equals $(48 + 50 + 64)/(48 + 50 + 64 + 8 + 100) = 3/5$.

The relative contributions of the $2P_{3/2}$ F=1/2, 3/2 excited state hyperfine levels to peak 6 was computed by taking the ratios of the excitation probability times the detected fluorescence signal. This is given by the following.

$$\frac{2P_{3/2} \;\; F = 1/2 \text{ contribution to Peak 6}}{2P_{3/2} \;\; F = 3/2 \;\; \text{contribution to Peak 6}} = \frac{4/9 \times 2/3}{5/9 \times 3/5} = 8/9$$

Hence, the fractions of peak 6 originating from the radiative decay of the $2P_{3/2}$ F=1/2, 3/2 hyperfine levels are 47.06% and 52.94%, respectively. The position of peak 6 relative to the $2P_{3/2}$ center of gravity was estimated by multiplying these fractions by the respective hyperfine level energies to give +1.970 MHz relative to the ^{6}Li $2P_{3/2}$ center of gravity.

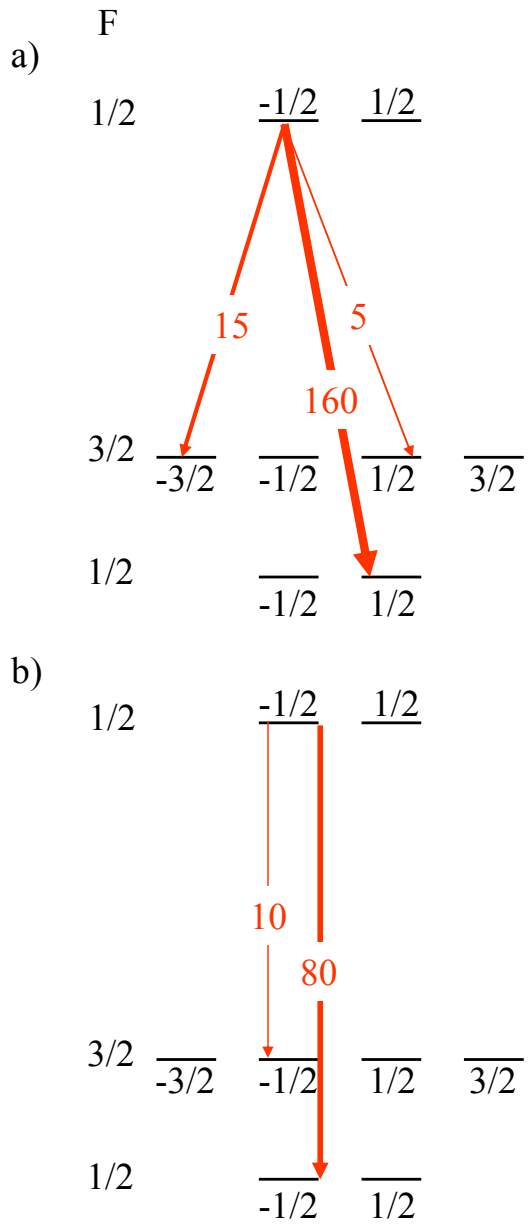

Figure C.2: Fluorescence Decay of ^{6}Li $2P_{3/2}$ F=1/2 $\rightarrow$ $2S_{1/2}$ Hyperfine Levels producing (**a**) circularly polarized and (**b**) linearly polarized fluorescence. The red numbers denote the relative branching ratio of the transitions found using the square of the dipole matrix element discussed in the text. For simplicity, decays are only shown for atoms initially occupying the $m_F = -1/2$ sublevel.

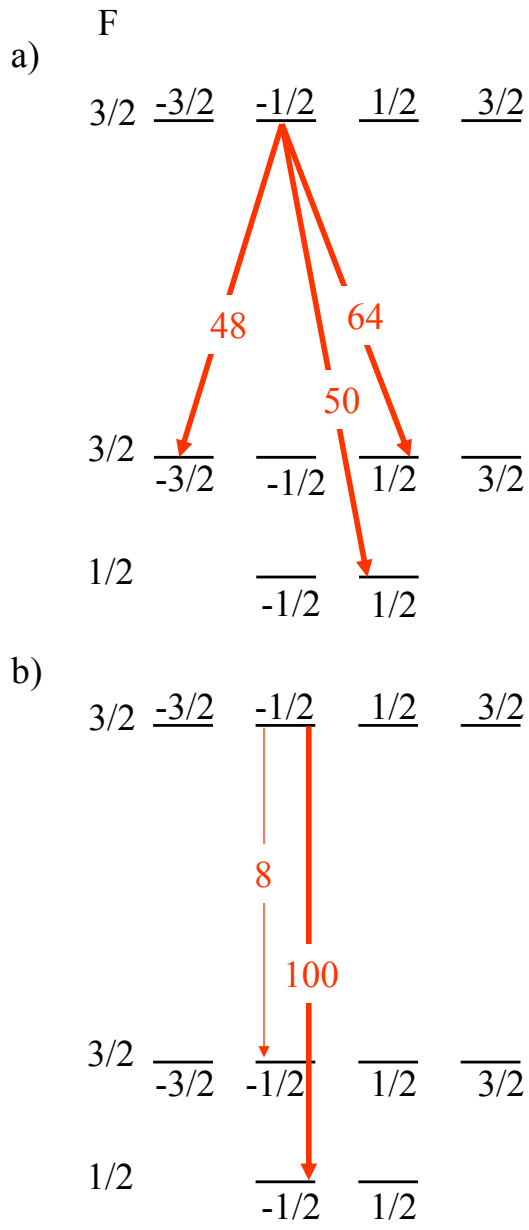

Figure C.3: Fluorescence Decay of ^{6}Li $2P_{3/2}$ F=3/2 $\rightarrow$ $2S_{1/2}$ Hyperfine Levels producing (**a**) circularly polarized and (**b**) linearly polarized fluorescence. The red numbers denote the relative branching ratio of the transitions found using the square of the dipole matrix element discussed in the text. For simplicity, decays are only shown for atoms initially occupying the $m_F = -1/2$ sublevel.

References

[1] R. C. Weast, *Handbook of Chemistry and Physics 69th Edition*, CRC Press, Boca Raton, 1988.

[2] F. Schmitt, A. Dax, R. Kirchner, H. J. Kluge, T. Kühl, I. Tanihata, M. Wakasugi, H. Wang and C. Zimmermann, *Hyperfine Interactions*, **127**, 111, 2000.

[3] G. J. Ritter, *Can. J. Phys.*, **43**, 770, 1965.

[4] H. Rong, S. Grafström, J. Kowalski, G. zu Putlitz, W. Jastrzebski and R. Neumann, *Z. Phys. D*, **25**, 337, 1993.

[5] E. Riis, A. G. Sinclair, O. Poulsen, G. W. F. Drake, W. R. C. Rowley and A. P. Levick, *Phys. Rev. A*, **49**, 207, 1994.

[6] J. J. Clarke and W. A. van Wijngaarden, *Phys. Rev. A*, **67**, 012506, 2003.

[7] K. C. Brog, T. G. Eck and H. Wieder, *Phys. Rev.*, **153**, 91, 1967.

[8] L. Windholz, H. Jäger, M. Musso and G. Zerza, *Z. Phys. D: At. and Mol. Clusters*, **16**, 41, 1990.

[9] W. Scherf, O. Khait, H. Jäger and L. Windholz, *Z. Phys. D: At. and Mol. Clusters*, **36**, 31, 1996.

[10] D. Das and V. Natarajan, *Phys. Rev. A*, **75**, 052508, 2007.

[11] J. Walls, R. Ashby, J. J. Clarke, B. Lu and W. A. van Wijngaarden, *Eur. Phys. J. D*, **22**, 159, 2003.

[12] H. Orth, H. Ackermann and E. W. Otten, *Z. Phys. A*, **273**, 221, 1975.

[13] C. Umfer, L. Windholz and M. Musso, *Z. Phys. D: At. and Mol. Clusters*, **25**, 23, 1992.

[14] C. J. Sansonetti, B. Richou, J. R. Engleman and L. J. Radziemski, *Phys. Rev. A*, **52**, 2682, 1995.

[15] B. A. Bushaw, W. Nörtershäuser, G. Ewald, A. Dax and G. W. F. Drake, *Phys. Rev. Lett.*, **91**, 043004, 2003.

[16] G. Ewald, W. Nörtershäuser, A. Dax, S. Götte, R. Kirchner, H. J. Kluge, T. Kühl, R. Sanchez, A. Wojtaszek, B. A. Bushaw, G. W. F. Drake, Z. C. Yan and C. Zimmerman, *Phys. Rev. Lett.*, **94**, 039901, 2005.

[17] R. Sánchez, W. Nörtershäuser, G. Ewald, D. Albers, J. Behr, P. Bricault, B. A. Bushaw, A. Dax, J. Dilling, M. Dombsky, G. W. F. Drake, S. Götte, R. Krichner, H. J. Kluge, T.Kühl, J. Lassen, C. D. P. Levy, M. R. Pearson, E. J. Prime, V. Ryjkov, A. Wojtaszek, Z. C. Yan and C. Zimmerman, *Phys. Rev. Lett.*, **96**, 033002, 2006.

[18] G. A. Noble, B. E. Schultz, H. Ming and W. A. van Wijngaarden, *Phys. Rev. A*, **74**, 012502, 2006.

[19] W. A. van Wijngaarden, *Can. J. Phys.*, **83**, 327, 2005.

[20] G. W. F. Drake, W. Nörtershäuser and Z. C. Yan, *Can. J. Phys.*, **83**, 311, 2005.

[21] I. Tanihata, T. Kobayashi, O. Yamakawa, S. Shimoura, K. Ekuni, K. Sugimoto, N. Takahashi, T. Shimoda and H. Sato, *Phys. Lett. B*, **206**, 592, 1988.

[22] C. W. de Jager, H. de Vries and C. de Vries, *At. Nucl. Data Tables*, **36**, 495, 1987.

[23] W. A. van Wijngaarden and G. A. Noble, *Lect. Physics Notes, Springer-Verlag*, **745**, 2008.

[24] E. Arimondo, M. Inguscio and P. Violino, *Rev. Mod. Phys.*, **49**, 31, 1977.

[25] J. Carlsson and L. Sturesson, *Z. Phys. D*, **14**, 281, 1993.

[26] W. R. Johnson, U. I. Safronova, A. Derevianko and M. S. Safronova, *Phys. Rev. A*, **77**, 022510, 2008.

[27] M. Weissbluth, *Atoms and Molecules*, Academic Press, New York, 1978.

[28] J. S. Townsend, *A Modern Approach to Quantum Mechanics*, University Science Books, Calfornia, 2000.

[29] W. R. Johnson, *Atomic Structure Theory*, Springer-Verlag, New York, 2007.

[30] G. W. F. Drake, *Atomic, Molecular & Optical Physics Handbook*, AIP Press, New York, 1996.

[31] B. H. Bransden and C. J. Joachain, *Physics of Atoms and Molecules*, Longham Inc., New York, 1983.

[32] Z. C. Yan and G. W. F. Drake, *J. Phys. B: At. Mol. Phys.*, **30**, 4723, 1977.

[33] G. W. F. Drake, *Advances in Quantum Chemistry*, **53**, 154, 2008.

[34] Z. C. Yan, W. Nörtershäuser and G. W. F. Drake, *Phys. Rev. Lett.*, **100**, 243002, 2008.

[35] M. Puchalski, A. M. Moro and K. Pachucki, *Phys. Rev. Lett.*, **97**, 133001, 2006.

[36] R. D. Knight and M. H. Prior, *Phys. Rev. A*, **21**, 1, 1980.

[37] G. C. Bjorklund and M. D. Levenson, *Appl. Phys. B*, **49**, 32, 145, 1983.

[38] G. C. Bjorklund and M. D. Levenson, *Phys. Rev. A*, **24**, 166, 1981.

[39] Arimondo et al [24] lists two different values, -0.010 ± 0.014 and -0.10 ± 0.14 MHz for $b(^6\mathrm{Li}\ 2\mathrm{P}_{3/2})$ as well as $b(^7\mathrm{Li}\ 2\mathrm{P}_{3/2}{=}{-}0.221 \pm 0.029$ MHz. The ratio of the ^{6}Li and ^{7}Li electric quadrupole constants should equal the ratio of the nuclear electric quadrupole moments whose magnitude has been found to be 0.023 [65], [7]. Hence, the correct value for $b(^6\mathrm{Li}\ 2\mathrm{P}_{3/2})$ is -0.010 ± 0.014 MHz.

[40] D. Das and V. Natarajan, *J. Phys. B*, **41**, 035001, 2008.

[41] K. Below and A. Derevianko, *Phys. Rev. A*, **78**, 032519, 2008.

[42] W. A. van Wijngaarden, *Advances in Atomic, Molecular & Optical Physics*, **36**, 305, 1996.

[43] J. J. Clarke and W. A. van Wijngaarden, *Recent Research Developments in Physics*, **3**, 347, 2003.

[44] Preliminary work described in the thesis of J. Walls [66] calibrated the laser scan using the ground state hyperfine splitting as measured by atomic clock [45].

[45] A. Beckmann, K. D. Böklen and D. Elke, *Z. Phys.*, **270**, 173, 1974.

[46] W. A. van Wijngaarden, *Proceedings of the 16th International conference on Atomic Physics*, **56396**, 1999.

[47] Edwards High Vacuum International, *Diffstak Mk 2 Diffusion Pumps Instructions Manual*, Edwards High Vacuum International, 1996.

[48] Edwards High Vacuum International, *RV3, RV, RV8 and RV12 Rotary Vane Pumps*, Edwards High Vacuum International, 1996.

[49] W. A van Wijngaarden and J. Li, *Phys. Rev. A*, **49**, 1158, 1994.

[50] Coherent Inc., *699 Series Ring Dye Laser Manual*, Coherent Inc.

[51] C. C. Bradley, C. A. Sackett, J. J. Tollett and R. G. Hulet, *Phys. Rev. Lett.*, **75**, 1687, 1995.

[52] New Focus, *Model Series 44xx and 485x Users Manual High-Frequency Electro-Optic Phase Modulators*, New Focus, Calfornia, 1990.

[53] Agilent, *Agilent E8241A/44A/51A/54A PSG Series Performance Signal Generator Manual*, Agilent Technologies.

[54] J. Xia and W. A. van Wijngaarden, *Applied Optics*, **36**, 24, 5905–5907, 1997.

[55] Tektronix, *User Manual, Tektronix, TDS5000 Series Digital Phosphor Oscilloscopes, 071-0876-02*, Tektronix, Oregon.

[56] H. J. Metcalf and P. van der Straten, *Laser Cooling and Trapping*, Springer, New York, 1999.

[57] X. X. Guan and Z. W. Wang, *Eur. Phys. J. D.*, **2**, 21, 1998.

[58] N. Yamanaka, *J. Phys. Soc. Jap.*, **68**, 8, 2561, 1999.

[59] M. Goedfroid, C.F. Fischer and P. Jönsson, *J. Phys. B*, **34**, 6, 1079, 2001.

[60] Z. C. Yan and G. W. F. Drake, *Phys. Rev. A*, **66**, 042504, 2002.

[61] G. A. Noble and W. A. van Wijngaarden, *In press*, *CJP*, 2009.

[62] S. C. Pieper and R. B. Wiringa, *Ann. Rev. Nucl. Part. Sci.*, **51**, 53, 2001.

[63] C. E. Simien, J. D. Gillaspy and C. J. Sansonetti, *ICAP Poster*, 2008.

[64] P. R. Bevington, *Data Reduction and Error Analysis for the Physical Sciences*, McGraw-Hill, Inc., New York, 1969.

[65] N. A. Schuster and G. E. Pake, *Phys. Rev.*, **81**, 157, 1951.

[66] J. Walls, *Measurement of isotope shifts, fine and hyperfine structure splittings of the lithium D lines*, Master's thesis, York University, Toronto, Ontario, 2001.